



SLHC-PP

DELIVERABLE REPORT

EU DELIVERABLE: 7.1.3

Document identifier:	SLHC-PP-7.1.3-1093334-v1
Contractual Date of Delivery to the EC	End of Month 30 (Sept. 2010)
Actual Date of Delivery to the EC	30/9/2010
Document date:	30/9/2010
Deliverable Title:	Construction of the plasma generator and sub-systems (e.g. 2Hz RF generator, hydrogen gas injection and pumping)
Work package:	WP7: Development of critical components for the injectors
Lead Beneficiary:	CERN
Authors:	list
Document status:	Released
Document link:	https://edms.cern.ch/document/1093334/1



SLHC - PP

Large Hadron Collider Upgrade Preparatory Phase

<http://cern.ch/slhc-pp>

EDMS nb. 1093334	Creation Date: 06-August-2010	Version: 1
	Last Update: 30/09/2010 14:53	Nb of pages: 39

This document can be found at:
<https://edms.cern.ch/document/1093334/1>

Construction of the plasma generator and sub-systems

Authors	Approved by	
E. Chaudet A. Castel J.-F. Ecarnot D. Faircloth G. Favre F. Fayet J.-M. Geisser M. Haase A. Habert J. Hansen S. Joffe M. Kronberger D. Kuchler J. Lettry D. Lombard A. Marmillon J. Marques Balula S. Mathot P. Moyret D. Nisbet M. O'Neil M. Paoluzzi L. Prever-Loiri J. Sanchez Arias C.-S. Schmitzer R. Scrivens D. Steyaert H. Vestergard M. Wilhelmsson		

Distribution List

This project has received funding from the European Community's Seventh Framework Programme (FP7/2007-2013) under the Grant Agreement n° 212114

History of changes

Version	Date	Responsible	Modification
0.1	2010-08-06	M. Kronberger	Creation of document
1.0	2010-09-27	M. Kronberger, J. Lettry	Full version
2.0	2010-09-28	M. Kronberger, J. Lettry	1 st review
3.0	2010-09-29	M. Kronberger, J. Lettry	2 nd review
4.0	2010-09-30	M. Kronberger, J. Lettry	3 rd review
5.0	2010-09-30	M. Kronberger, J. Lettry	Final version

Abstract.

R & D for a Superconducting Proton Linac (SPL) at CERN is pursued in view of a possible application as proton driver for a future neutrino facility as well as a back-up plan for the LHC injectors in the context of the LHC luminosity upgrade (SLHC). In its high power version, the SPL requires an H⁻ source operating with a duty factor of up to 6 %, far beyond the capability of the present Linac4 source which operates only at ~0.1% duty factor. For this reason, an RF driven, non-cesiated plasma generator prototype for H⁻ production has been developed that will supersede the Linac4 source during SPL operation. This plasma generator has been designed to operate at a maximum RF power of 100kW and at duty factors of up to 6%. In this deliverable report, the construction of the plasma generator and its subsystems is outlined, and a description of the test arrangement is given.

1. Introduction

The RF-driven non-cesiated DESY-Linac4 H⁻ source [1] has been installed last year at the Linac4 test stand and is now being commissioned at a bias voltage of 45kV. The RF power used to generate and heat the plasma is supplied by an external antenna that operates in pulsed mode at a frequency close to 2MHz. At Linac4, this antenna will deliver up to 100kW of pulsed RF power in order to achieve a nominal H⁻ current of 80mA. The length of the RF pulse is 400 μ s, corresponding to a maximum duty factor of 0.08% for a repetition rate of 2Hz (Table 1).

As shown in an earlier study [2,3], the resulting maximum average heat load of 80W is already close to the limit of operation for some of the components of the Linac4 source. For this reason, a major effort has been taken in order to design a plasma generator that can operate in the high power (HP) mode of SPL, where duty factors of up to 6% will be reached.

Table 1: H⁻ source nominal operation parameters at Linac4 and SPL. The operation mode of the DESY-HERA RF source – the predecessor of the Linac4 source – is shown for comparison.

	Linac4	LP-SPL	HP-SPL	DESY
H ⁻ current [mA]	80	80	80	40
RF peak power [kW]	100	100	100	30
RF frequency [MHz]	2	2	2	2
repetition rate [Hz]	2	2	50	3
pulse length [ms]	0.4	0.9	0.4 - 1.2	0.15
duty factor [%]	0.08	0.18	2 – 6	0.045
Average RF power [W]	80	180	2000 - 6000	13.5

The improvements required to upgrade the plasma generator of the Linac4 H⁻ source have been identified and summarized in [4]. In line with this, a design strategy was developed for the implementation of these upgrades into the source. The main items of this design strategy are summarized below:

- Partitioning of the plasma generator into four independent sub-assemblies with different functionality to facilitate the development process.
- Production of a parameterized CAD model in order to allow for fast production of plasma generator models for input in various simulation tools, such as ANSYS and Opera.

- Replacement of materials used in the Linac4 source by materials with better heat conductivity, in particular where a good thermal flow is required.
- Optimization of the heat flow by:
 - a) upgrading the design of critical components to achieve a better heat conduction, and
 - b) improving thermal contact conductance by increasing contact surface areas, and by the brazing of conductors on insulators.
- Implementation of dedicated cooling circuits for the H₂ gas injection and plasma ignition region, the ceramic plasma chamber, the extraction region, and the antenna.
- Optimization of the cusp and filter field strength and uniformity by an electromagnetic (EM) study of the plasma generator.
- Minimization of ohmic losses in cusp magnets, ferrites, and metallic source components.
- Validation of the changes by CFD, EM and thermal-structural modeling.

Following this line, a model of a plasma generator was developed that is capable of operating in the HP-SPL mode [5,6]. This model served as a base for the production of the prototype that is presented in this report.

2. Design of the SPL plasma generator

Presentation of the fully assembled SPL PG

Fig. 1 shows a 3D CAD view of the SPL plasma generator prototype. Fig. 2 shows the plasma generator prototype after assembly at the CERN workshop.

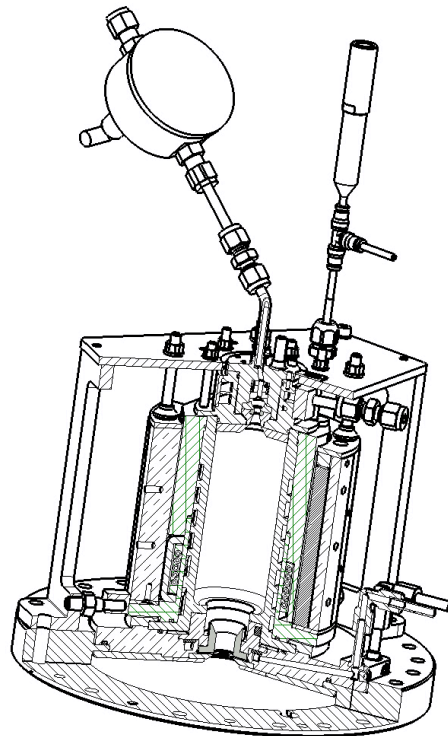


Figure 1: 3D view of the SPL plasma generator prototype.

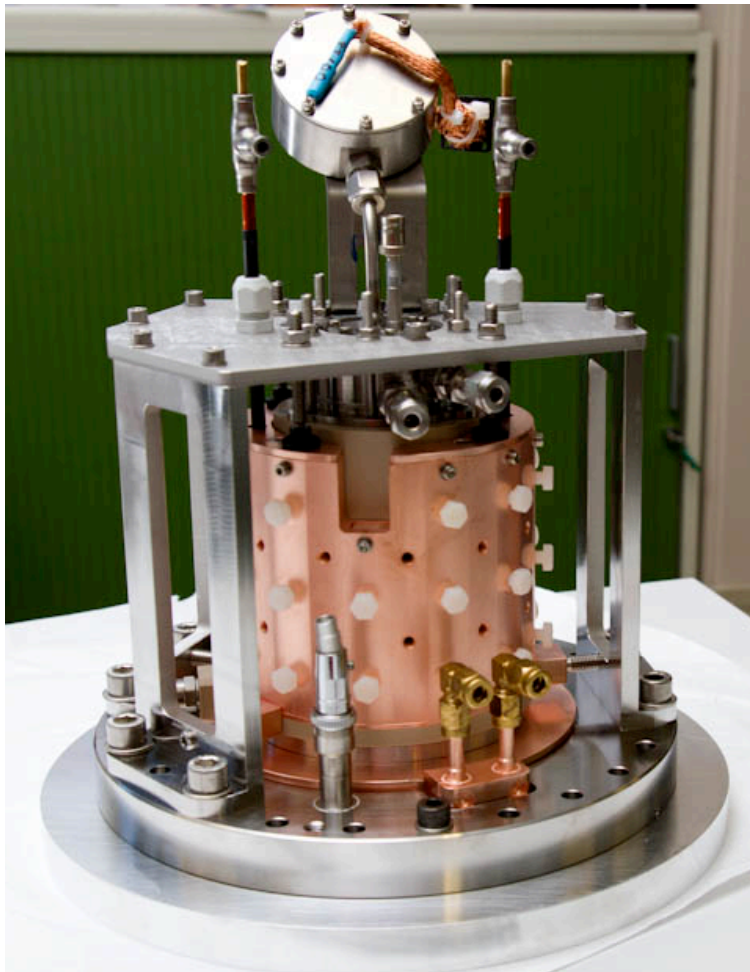


Figure 2: Assembled SPL plasma generator.

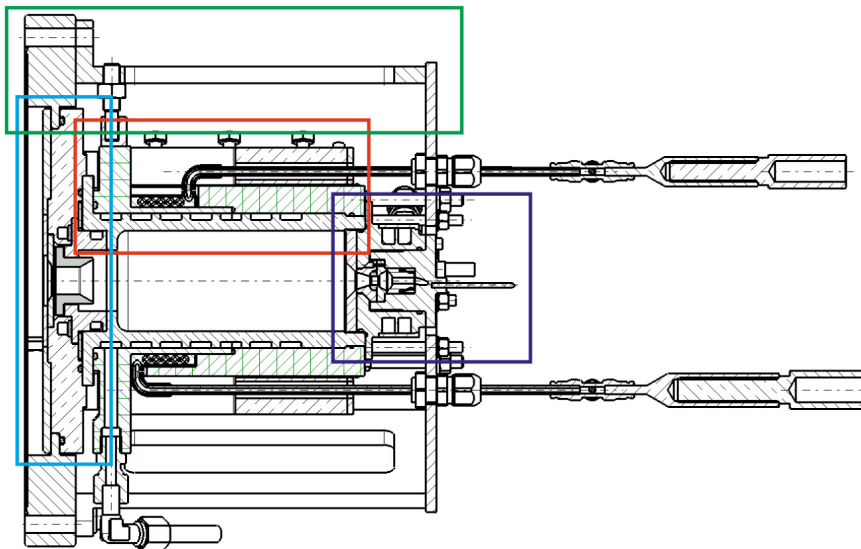


Figure 3: Cross-sectional view of the SPL plasma generator. The sub-assemblies of the plasma generator are indicated by colored rectangles. **Purple:** H₂ gas injection and ignition. **Red:** plasma chamber sub-assembly. **Blue:** extraction region. **Green:** Mechanical support.

A cross-sectional view of the plasma generator is shown in Fig. 3. The sub-assemblies of the plasma generator are indicated by colored rectangles. The following color scheme is used:

- **Purple:** H₂ gas injection and ignition.
- **Red:** plasma chamber and magnet cage.
- **Blue:** extraction region.
- **Green:** mechanical support.

In the following, the sub-assemblies of the plasma generator are presented and the changes since the last report are discussed.

3. Sub-assembly A: H₂ gas injection and ignition

General outline

The technical drawing and a photo of the H₂ gas injection and ignition sub-assembly are shown in Figs. 4 and 5. It is an upgraded version of the Linac4 design. The most important changes involve a more efficient electrode configuration, an axisymmetric gas injection, the use of AlN ceramic instead of Macor for the electrically insulating components, and a cooling circuit to remove the thermal load from the plasma and the plasma ignition (see [5] for details).

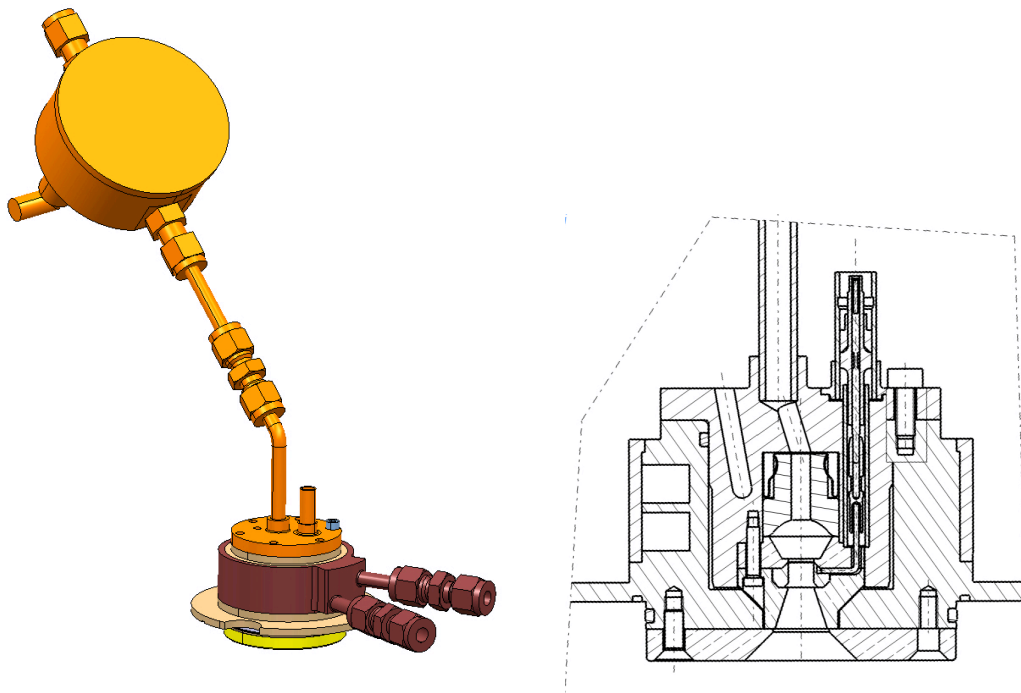


Figure 4: 3D view (left) and cross-section (right) of the H₂ gas injection and ignition sub-assembly.

Design changes since the previous deliverable report

The following components of the sub-assembly have been changed since the last report [5]:

- The stainless steel pipe between the piezo gas valve and the ignition element body has been extended to avoid possible sparking between the valve and

the electrical connectors of the antenna. This extension can be exchanged by a T piece onto which a pressure gauge can be mounted.

- In order to stabilize DC and pulsed mode gas injection, the temperature of the piezo gas valve is now regulated by means of an external cooling system (Fig. 5). This system consists of two Cu plates put on each side of the piezo gas valve and coupled to a cooling circuit. A thermostat (Lauda Alpha RA8) is used to regulate the temperature of the valve to $< 0.1^{\circ}\text{C}$ precision.

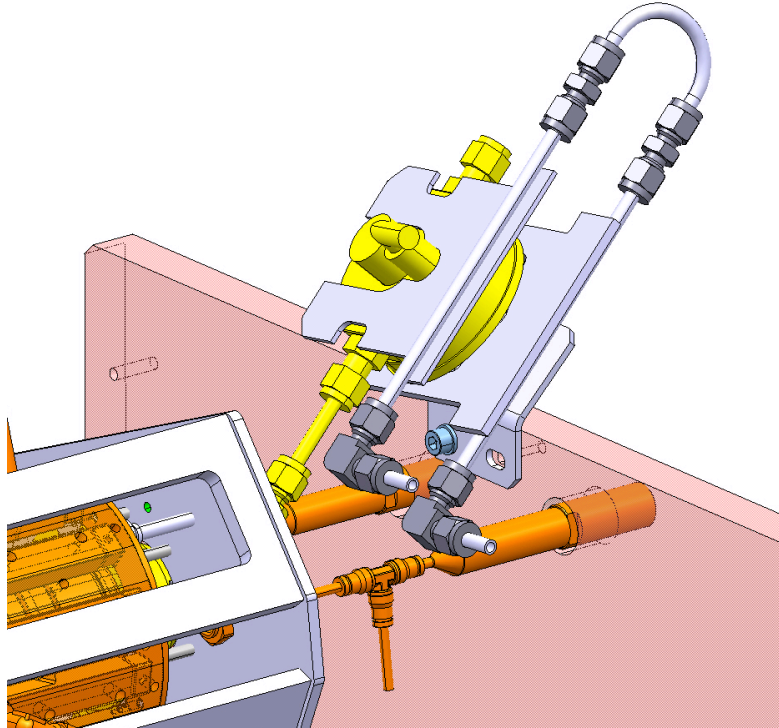


Figure 5: 3D view of the piezo gas valve equipped with the external temperature control system.

Production

Except from the AlN ceramics and the connectors, all components were produced at the CERN workshop. The AlN ceramics were produced by an external manufacturer¹.

4. Sub-assembly B: plasma chamber

The technical drawing and an image of the plasma chamber sub-assembly are shown in Figs. 6 and 7. It consists of the following main entities:

- the ceramic plasma chamber and associated cooling system;
- the RF antenna; and
- the magnet cage, including the cusp magnets, the ferrites, and their supporting structure.

¹ CeramTec AG, CeramTec-Weg 1, 95615 Marktredwitz, Germany

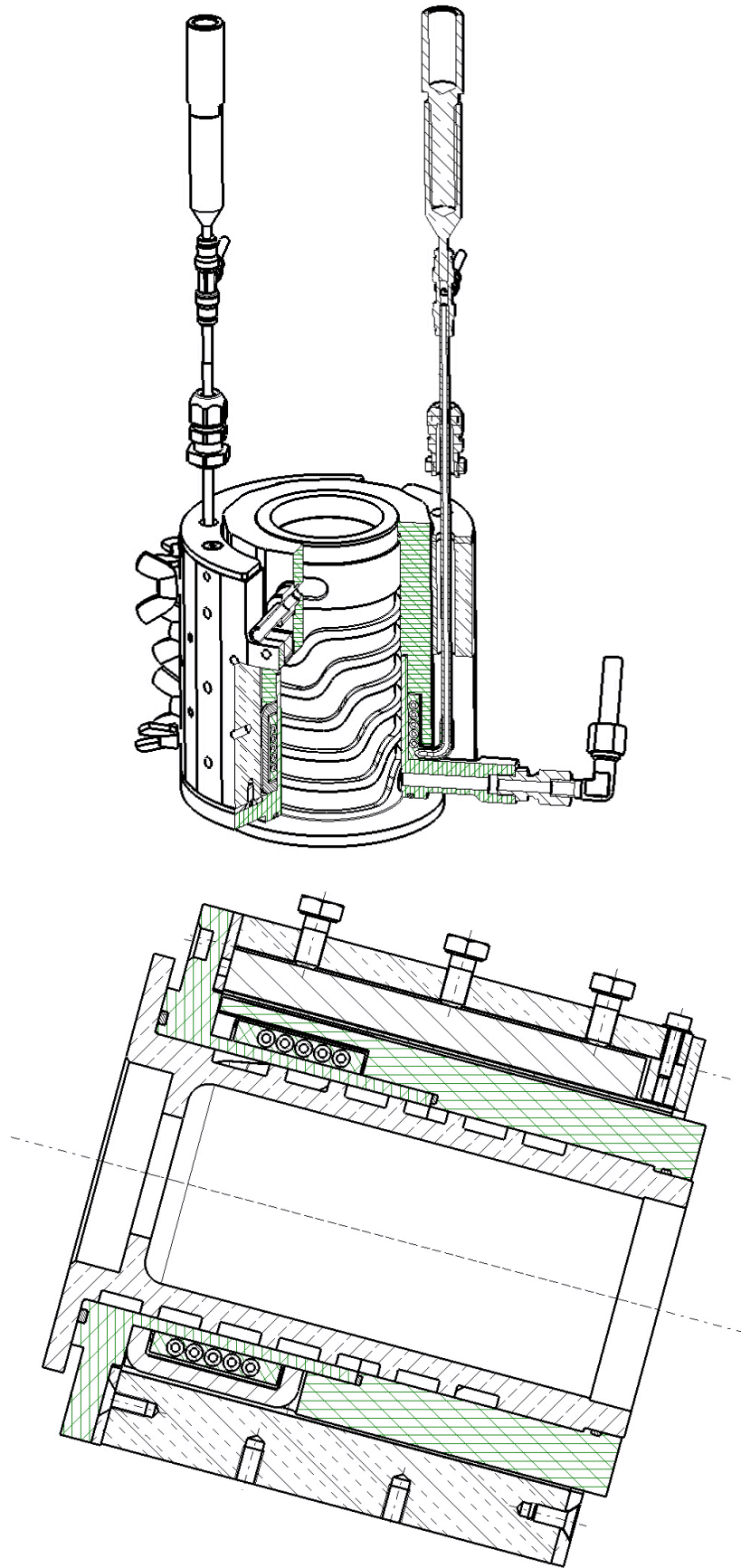


Figure 6: 3D drawing (top) and cross-section (bottom) of the plasma chamber sub-assembly.

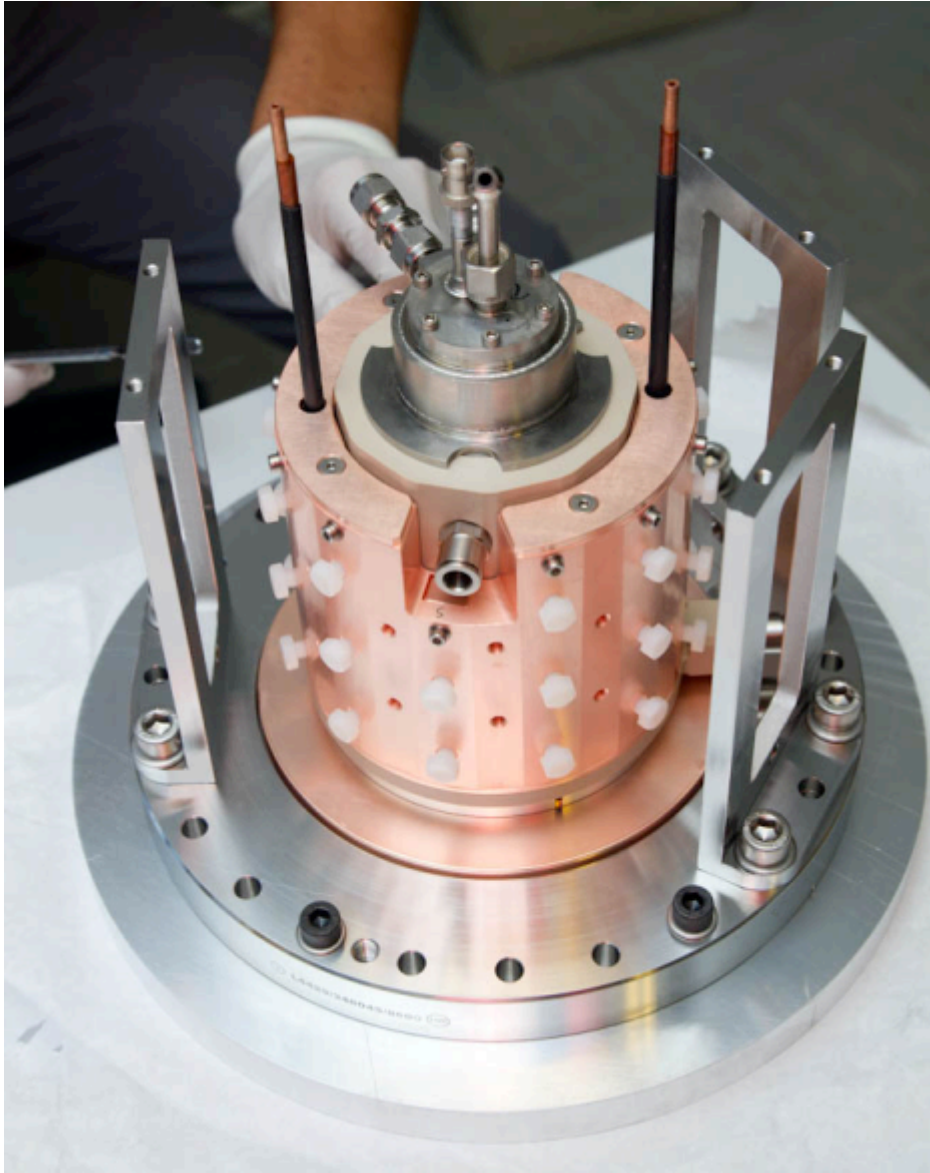


Figure 7: View of the assembled plasma chamber and ignition element.

4.3. Ceramic plasma chamber and cooling circuit

General outline.

A 3D view of the ceramic plasma chamber and the adjacent components is shown in Fig. 8. A comparison with the Linac4 plasma chamber is given in [5]. The new design comprises an outer flange at the front end that simplifies the assembly with the extraction collar, and an inner flange partially shielding the collar region from the plasma heating region (Fig. 6). The inner volume of the SPL plasma chamber is identical to its Linac4 counterpart, except from a 4% reduction in length. The exterior surface of the ceramic plasma chamber contains a coil-like cooling circuit for optimized cooling of the chamber even during operation at high duty factors and high RF power [5].

The ceramic plasma chamber is surrounded by a jacket or sleeve made of Polyether ether ketone (PEEK) that confines the cooling circuit on the outside. The PEEK

cooling sleeve is split into a front part and a back part in order to allow for the antenna to be installed. Connections for the cooling water inlet and outlet are implemented at the front and back end of the sleeve. The leak tightness of the cooling circuit is assured by three o-ring seals (one at the back end, one at the front end and one at the contact surface between the front and back part).

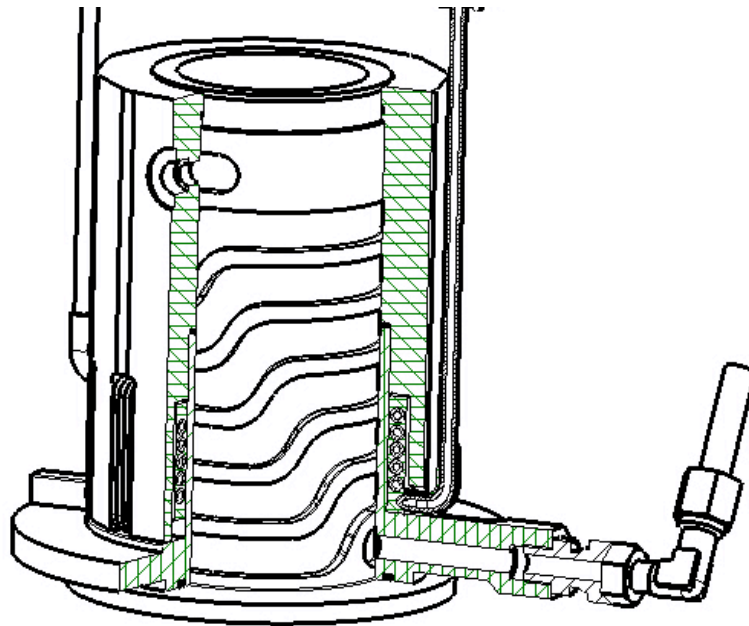


Figure 8: 3D drawing of the ceramic plasma chamber and PEEK cooling sleeve.

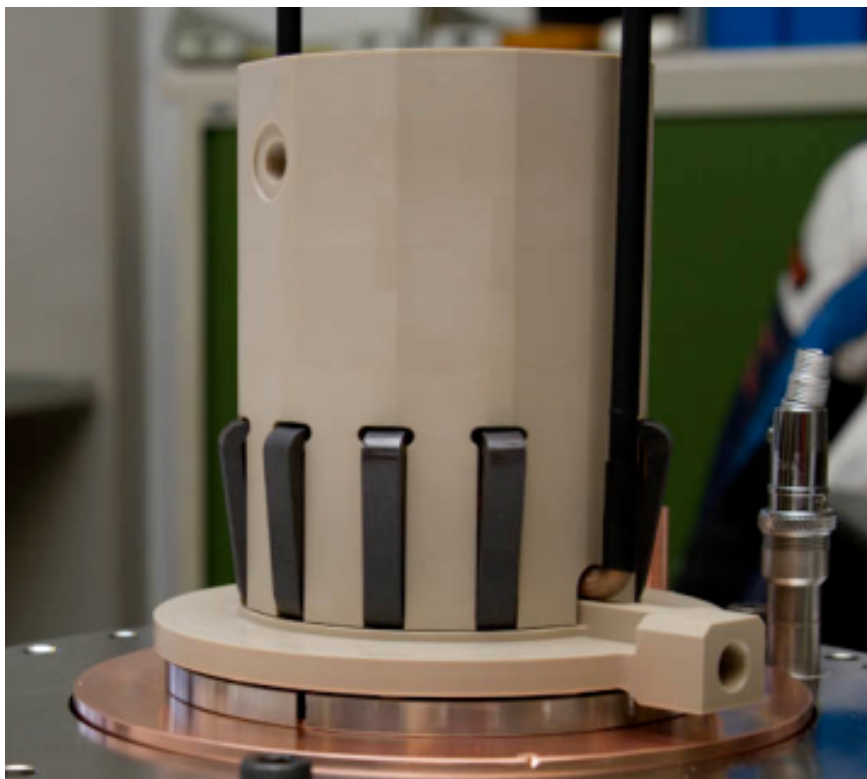


Figure 9: Ceramic plasma chamber, cooling sleeve, and ferrites during assembly.

Design changes since the previous deliverable report.

Ceramic plasma chamber:

Only small changes have been applied to the ceramic plasma chamber:

- The thickness at the back end has been increased. This makes a re-location of the o-ring seal with sub-assembly A (H_2 gas injection and ignition) possible, in case that difficulties with the current solution occur during assembly.
- The location of the o-ring seal at the back end has been changed slightly (see also below)
- The cooling circuit has been extended slightly at the outlet in order to achieve an angle between cooling circuit inlet and outlet of exactly 90 degrees.

PEEK cooling sleeve:

Major modifications were done on the PEEK cooling sleeve, mostly due to the changed design of the magnet cage (see Sect. 4.5).

- *Front end part:* The foremost section has been radially extended to account for the increased size of the new magnet cage. The cooling circuit inlet section has been designed more robust in order to facilitate the implementation of the connection with the water pipe.
- *Back end part:* Thickness and size along the axis have increased significantly, improving the robustness of the piece and facilitating the implementation of the cooling circuit outlet. Notches hosting the ferrites have been added at the front end. An o-ring groove has been implemented at the back end of the sleeve. The exterior surface is of polygonal shape which helps in the positioning of the Cu cage.

Production

Two ceramic plasma chambers made of AlN ceramic have been produced externally by CeramTec (Fig. 10). Several non-critical flaws (sharp edges at cooling channels, deviations of the cooling channel shape from nominal, surface roughness) were detected during inspection at CERN on the produced specimen. The flaws were discussed with the producer, and a strategy for mitigation in future chambers developed. This strategy involves minor design adaptations on the outline of the cooling circuit, and changes in the manufacturing process itself. The PEEK cover was produced at the CERN workshop.



Figure 10: Installed AlN ceramic plasma chamber.

4.4. RF antenna and ferrites

General outline

The technical drawing of the RF antenna of the SPL plasma generator prototype is shown in Fig. 11. An image of the produced antenna is provided in Fig. 12. The inner and outer radii of the antenna are 35mm and 40 mm, respectively. In contrast to the RF antenna of the Linac4 source, it is made of hollow-tube Cu with 4mm outer diameter and 2mm inner diameter in order to be able to cool the antenna internally during operation. The antenna currently installed in the plasma generator prototype has 5 ½ windings, equivalent to the Linac4 antenna. A stacked antenna with up to 10 windings may be used in future experimental runs. Ferrites surrounding the antenna coil are used to enhance coupling of the RF field into the plasma.

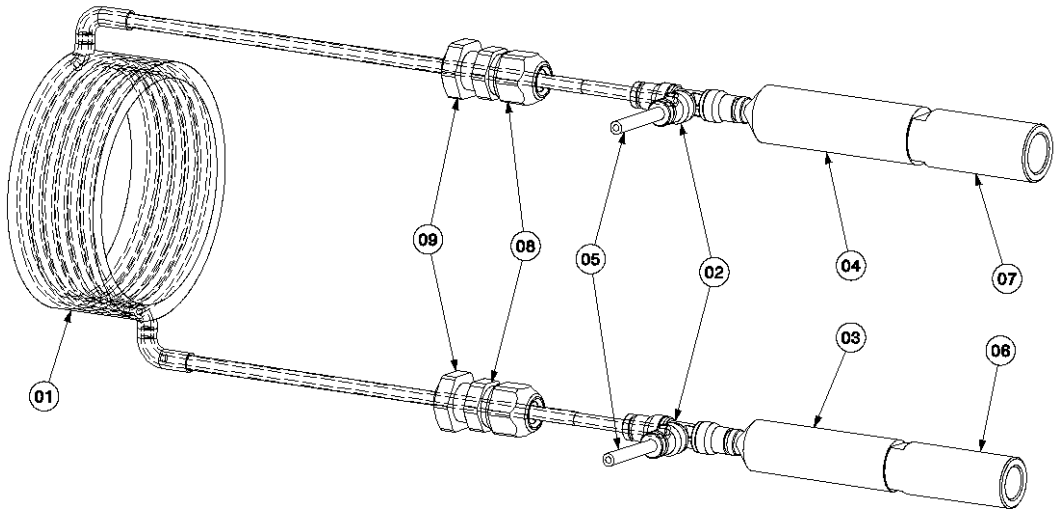


Figure 11: 3D technical drawing of the antenna. (1) epoxy-molded antenna coil. (2) cooling T connectors. (3) + (4) asymmetric RF connectors (female). (5) water connections. (6) + (7) asymmetric RF connectors (male). (8) + (9) insulated antenna feed-through.

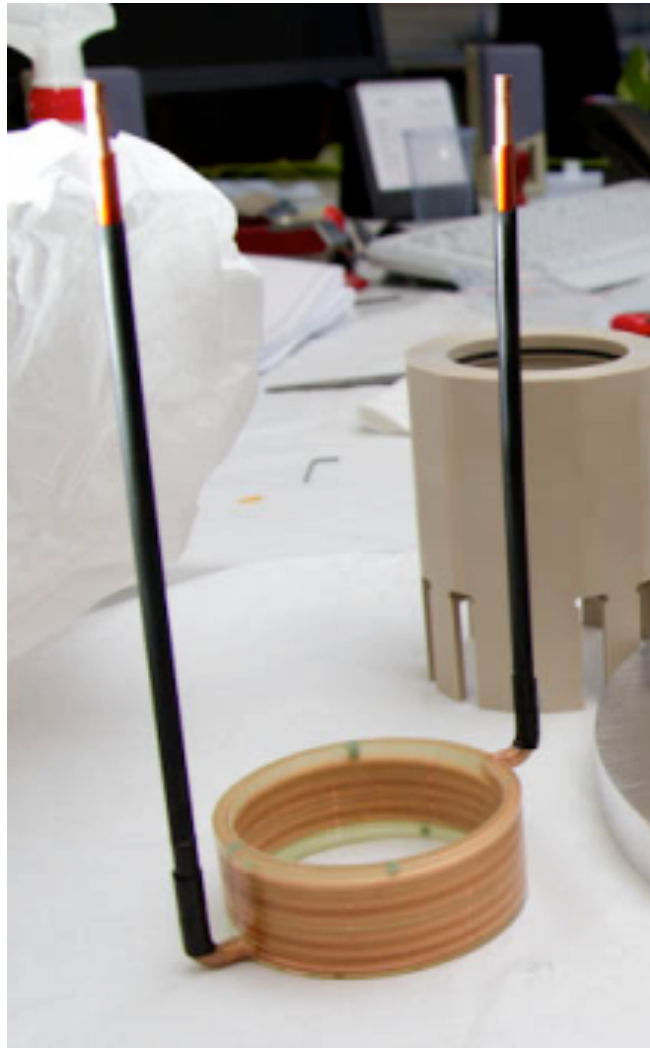


Figure 12: Photo of the installed RF antenna.

Design changes since the previous deliverable report

RF antenna:

- The insulation of the RF antenna is an epoxy cylinder into which the antenna coil is embedded, improving the rigidity and mechanical stability of the coil.
- In order to avoid sparking between the antenna tips and the Cu magnet cage, the antenna tips are insulated each by 0.3 mm of Kapton tape and additional shrink tubes with thickness 0.5mm, giving a total dielectric strength > 50 kV.
- Simultaneous supply with cooling water and electrical power is achieved by T-connectors at the end of the antenna tips.

Ferrites:

- The shape of the ferrites was changed in order to reduce the heat load on the magnets and, to maximize the magnetic field strength inside the plasma chamber. Two ferrites are shown in Fig. 13.
- Two different sets of ferrites are available:
 - Width = 8mm, Material: 4L, FerroXCube² (see Fig. xxx)
 - Width = 2.55mm, Material: 8C11, FerroXCube²

Having two sets of ferrites allows for comparing the impact of different ferrite materials on the RF coupling. In addition, the latter set of ferrites can also be used for an evaluation how the coupling of RF power into the plasma changes with increasing amount of ferrite material surrounding the antenna.

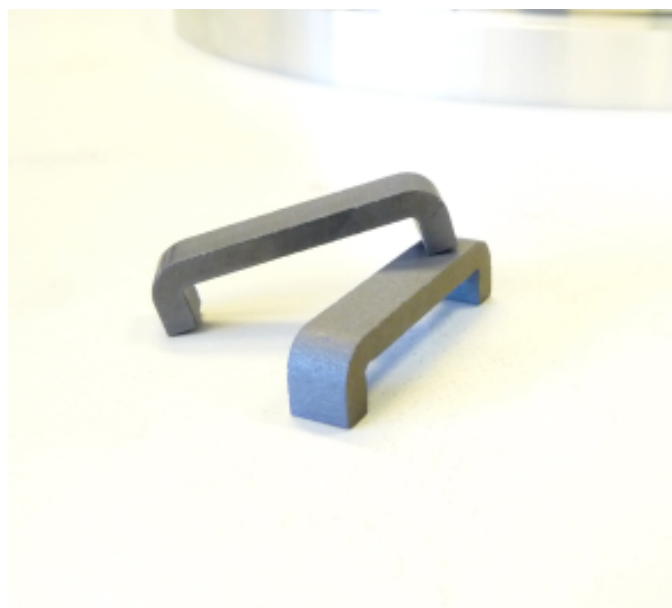


Figure 13: Two of the ferrites used in the SPL plasma generator.

Production:

The antenna was crafted at the CERN workshop using a dedicated winding tool. The molding of the RF antenna epoxy insulation was processed and optimized at CERN. To optimize antenna uniformity and assure a minimum dielectric strength of the insulation of 8kV, the windings were separated by thin (0.3mm) intermediate epoxy disks before molding in order to avoid shortcuts resulting from direct physical contacts between two or more windings. Additional epoxy sheets of the same thickness were placed at the front and back ends and the inner and outer diameter of the antenna coil. The antenna shape was optimized by small epoxy blocks. The

² FerroXCube, Hamburg, Germany

molding procedure was tested on several antenna prototypes in order to exclude enclosed air bubbles.

The 8C11 ferrites were purchased from FerroXCube. The 4L ferrites were produced at CERN from available spares.

4.5. Magnet cage

The magnet cage of the SPL plasma generator has seen the most significant changes of all source components. The changes were motivated by:

- (a) the optimization of the magnetic configuration,
- (b) the minimization of power losses due to eddy currents induced by the RF field.

In the following, these two issues are briefly reviewed, and the final design of the magnet cage is described.

Magnetic cusp configuration of the SPL plasma generator

The magnetic cusp field is a multipole magnetic configuration around the plasma chamber of an ion source plasma chamber. It reduces the plasma losses on the chamber walls, thus reducing heat loads and increasing the plasma density. In order to optimize the plasma production by the RF-coil, the gradient of the magnetic field strength should be high close to the walls of the plasma chamber in order to maximize the volume where the magnetic field strength is low. Furthermore, the magnetic field strength close to the wall should be as high as possible for optimum wall protection. For this reason, a dodecapole magnetic configuration was chosen.

To determine the size, type and configuration of the cusp field, simulations with the TOSCA module of Vector Fields Opera© were performed. In order to make the cusp field comparable with Linac4, it was aimed to achieve for the SPL plasma chamber cusp field a similar magnetic field strength and orientation in the region of the plasma chamber wall (maximum B_t) and plasma area as in the Linac4 source. However, due to the increased thickness of the ceramic plasma chamber and the cooling sleeve, the magnets have to be mounted at a larger radial distance from the center (46mm compared to 35mm in the Linac4 source) which would result in a drastic decrease of magnetic field strength, if the same type of magnets as in Linac4 would be used.

As the mechanical constraints prohibit a sufficient increase of magnet size, a dodecapole magnetic cusp configuration employing offset-Halbach-type magnets was introduced (Fig. 14; see also [5]). Each individual Halbach element consists of 3 magnets of size $4.5 \times 10 \times 99 \text{ mm}^3$, giving a total size per Halbach element of $13.5 \times 10 \times 99 \text{ mm}^3$.

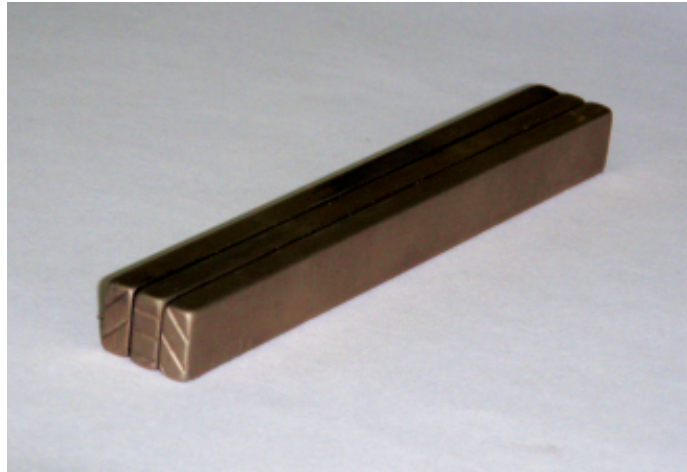


Figure 14: Photograph of an offset Halbach element.

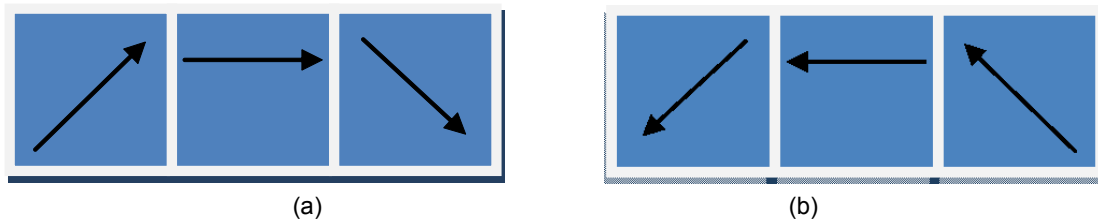


Figure 15: Scheme of an offset Halbach element. (a) clockwise orientation. (b) counterclockwise orientation. The arrows indicate the direction of magnetization.

As can be seen in Fig. 15, a Halbach element can be oriented such that the magnetization vectors point in clockwise (cw) or counterclockwise (ccw) direction. In order to create the multipole cusp configuration, cw and ccw oriented Halbach elements are alternately positioned around the plasma chamber. Between the Halbach elements, the magnetic field is purely radial and the U-shaped ferrites reinforce these radial components.

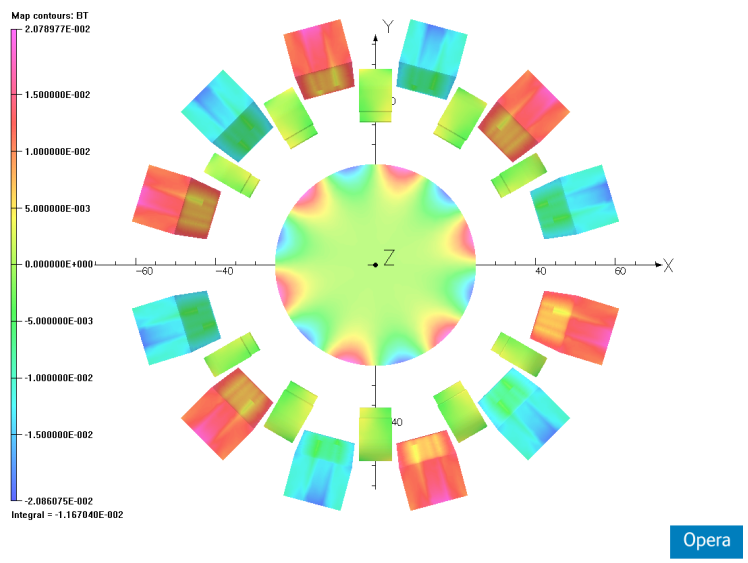


Figure 16: magnetic cusp configuration of the SPL plasma generator. Ferrites are shown in green, which cw and ccw oriented Halbach elements are shown in red and turquoise, respectively. The circular inset shows the tangential magnetic field B_t inside the plasma region and at the center of the antenna.

Fig. 16 shows the magnetic cusp configuration of the SPL plasma generator. The circular inset depicts the tangential magnetic field B_t inside the plasma region and at the center of the antenna coil. Note that two of the cusp magnets are shorter than the remaining ones (70mm instead of 99mm length) due to space restrictions by the plasma chamber cooling outlet and symmetry considerations. Ferrites are missing in two positions due to the presence of the antenna tips.

The variation of B_t along the plasma chamber wall is shown in Fig. 17. Small perturbations of the maximum field strength in the range of $\pm 5\%$ are present and due to the missing ferrites.

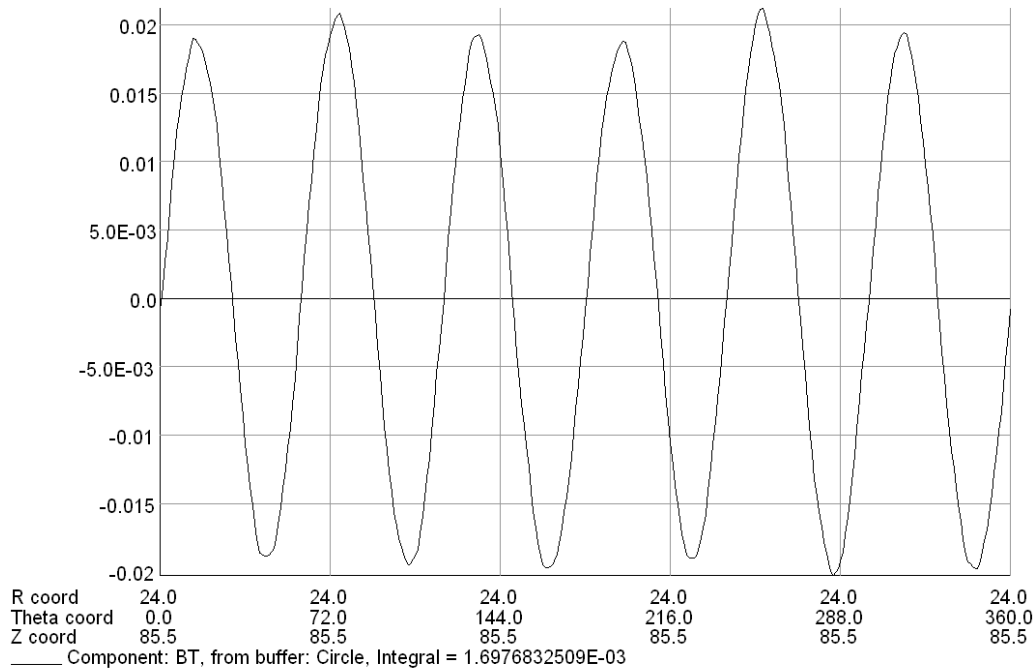


Figure 17: tangential magnetic field B_t at the plasma chamber wall at the position of the antenna coil. Ordinate: magnetic field in Tesla.

Fig. 18 plots B_t versus the radial distance from the center along a line connecting two magnets. The magnetic field strength at the chamber wall is approximately 20mT and drops to below 0.1mT in the center.

In addition to the Halbach elements, brick-shaped magnets with standard N-S magnetization and respective sizes $13.5 \times 10 \times 99 \text{ mm}^3$ and $13.5 \times 10 \times 70 \text{ mm}^3$ have been purchased. These magnets will produce a $\approx 40\%$ weaker dodecapole field as the Halbach elements and will be used to assess the dependence of plasma parameters on the strength of the magnetic cusp field.

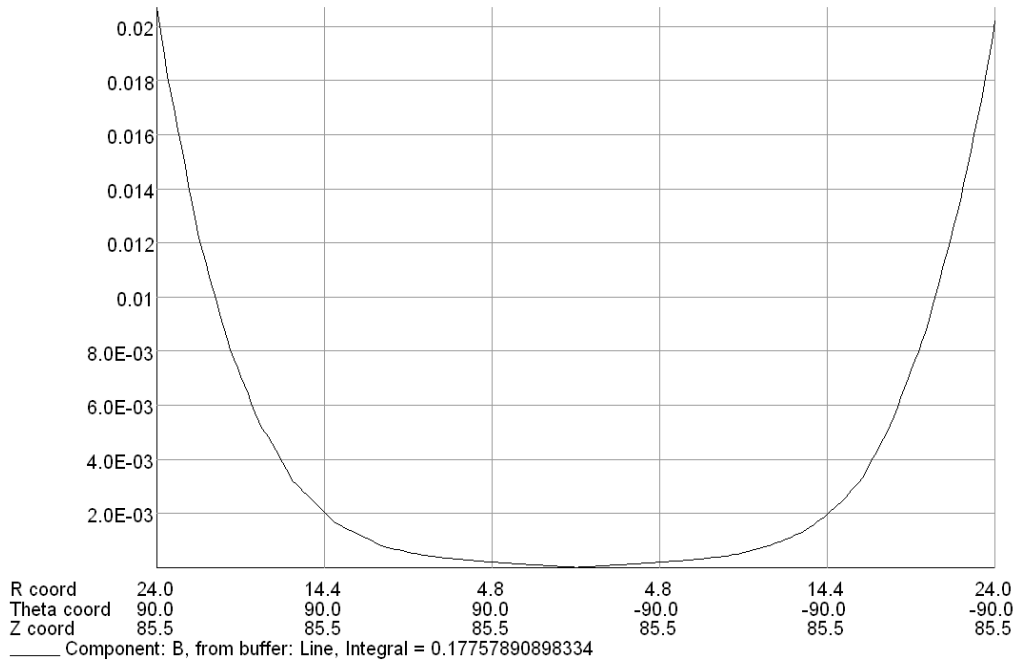


Figure 18: Radial plot of total magnetic field across the plasma chamber. Units of abscissa and ordinate are mm and Tesla, respectively.

4.6. Electromagnetic (EM) modeling of the SPL plasma generator

Initial EM modeling of the SPL magnetic configuration

The dissipation of RF power induced by eddy currents in the magnetic components of the SPL plasma generator was studied by a simplified EM model with the Vector Fields Opera software package (Fig. 19). The model consisted of four different components: the RF antenna, a NdFeB permanent magnet (Vacuumschmelze, Vacodym 633HR), the plasma, and an optional NiZn ferrite (FerroXCube, type 8C11). To reduce computational power, a mirror-symmetric model with 2 x ½ permanent magnet and 2 x 1 ferrite was simulated.

The RF antenna was modeled as a cylindrical Biot-Savart type conductor with 5.5 turns, inner and outer radii of 35.5mm and 39.5mm, respectively, and a winding length of 28mm. The peak antenna current I_{peak} was set to 350A, which is the value for 100kW operation extrapolated from measurements at Linac4. The sizes, shapes and positions of the magnets and ferrites corresponded to the SPL plasma generator magnetic configuration, except from the magnet length (43mm). The plasma was modeled as a cylindrical body with a length of 45mm and a diameter of 48mm. In order to optimize calculation time, only 1/8 of the model was simulated and the remaining parts taken into account by symmetry planes.

Special care was taken to model the ferrites, magnets and the plasma as realistic as possible. Relevant electromagnetic properties of the ferrites, NdFeB and the plasma are given in Table 2 for a frequency $f = 2\text{MHz}$. The properties of the ferrites and NdFeB magnets were taken from data sheets provided by the suppliers. Hysteresis losses of the ferrites were not taken into account. The relative permeability μ_R of the magnets was set to 1 to account for the saturation of the material when magnetized. The thin Ni coating of the magnets was not taken into account in the simulations as

the skin depth δ exceeds the thickness of the layer ($\approx 10\mu\text{m}$) by one order of magnitude at saturation. The values of μ_R and δ of the plasma were derived from measurements performed at the Linac4 source. No value of μ_R is given for the ferrites due to the non-linearity of the hysteresis. The skin depths of the materials were calculated from equation (1):

$$\delta = \frac{1}{\sqrt{\pi f \mu_0 \mu_r \sigma}}, \quad (1)$$

with the magnetic constant, $\mu_0 = 4\pi \times 10^{-7} \text{H/m}$, and the electrical conductivity σ . The average power dissipation P_{diss} per surface S over an ac cycle was calculated by

$$P_{diss} = \frac{R_s}{2} \int_S H^2 dS \quad (2)$$

where R_s is the surface resistance,

$$R_s = \frac{1}{\sigma \delta} \quad (3)$$

and H the magnetic field strength. For a given frequency f and magnetic field strength H , P_{diss} scales therefore with the square root of $\mu_R \cdot \sigma$.

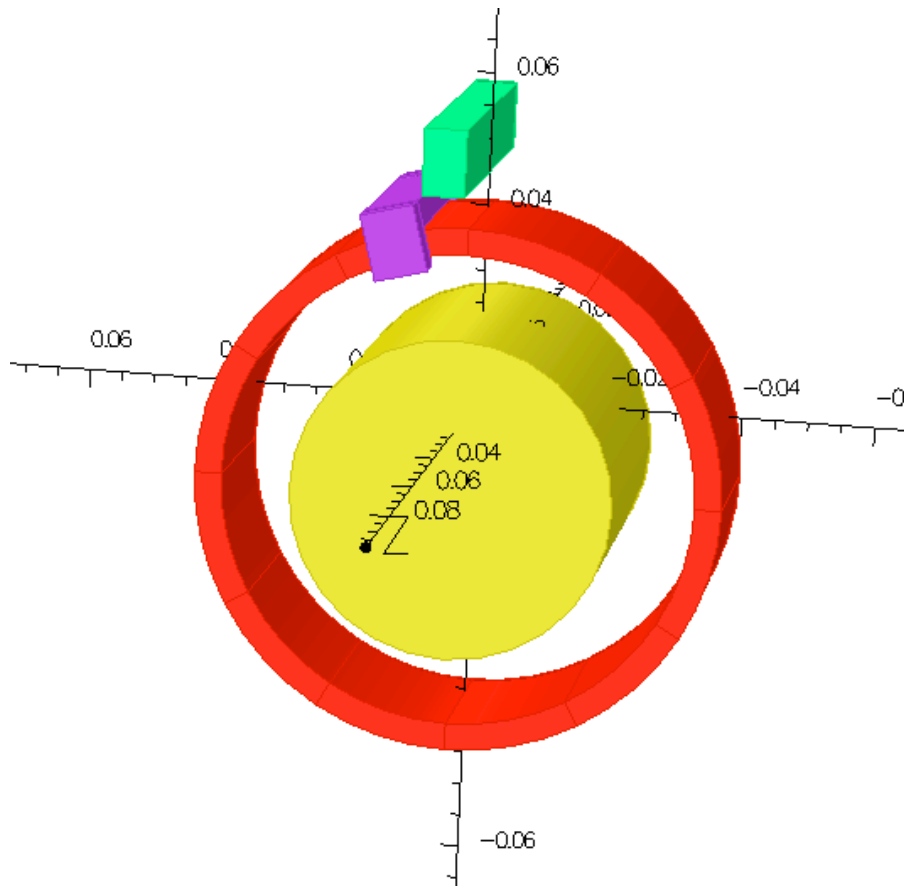


Figure 19: Simplified model of the SPL plasma generator with unshielded magnets. **Red:** RF antenna. **Yellow:** plasma cylinder. **Green:** NdFeB magnet. **Purple:** Ferrite.

Table 2: Skin depths δ calculated for the materials in the simplified source at $f = 2\text{MHz}$.

	NdFeB	Nickel	Copper	Ferrite	Plasma
μ_r (Typical)	1	1	1	Variable	0.92
σ (Sm^{-1})	6.67×10^5	1.40×10^7	6.0×10^7	1.0×10^{-5}	30
δ (μm)	440	95	46	$\approx 10^6 - 10^7$	7×10^4

Fig. 20 shows a comparison of the B field distribution for a simulated system with ferrite and one without ferrite. Due to the high field strengths close to the antenna, most of the volume of the ferrite is saturated. Nevertheless, the presence of the ferrites reduces the field strength seen by the magnets significantly.

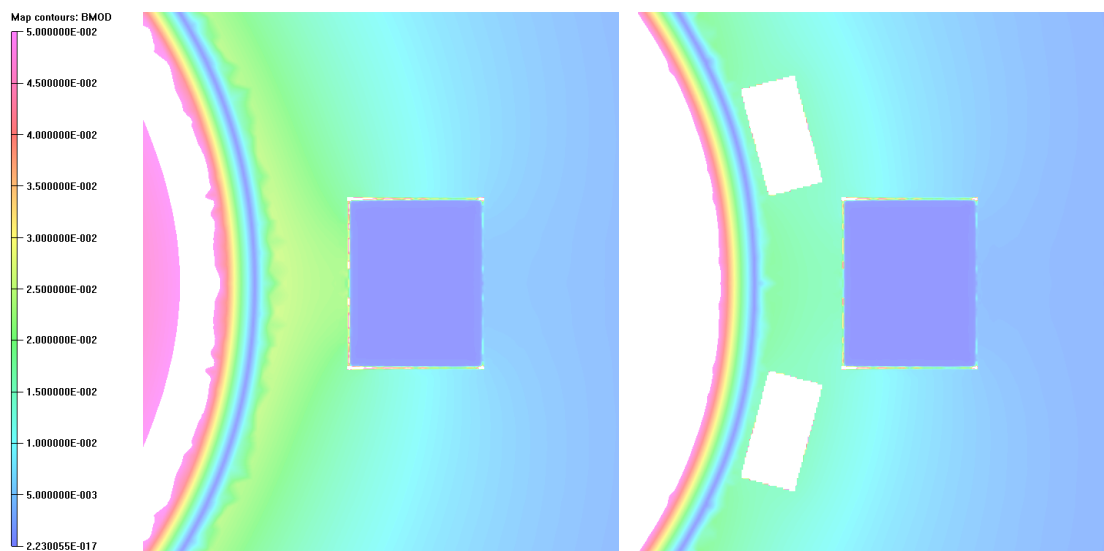


Figure 20: B field distribution for the simplified simulated system. Left: no ferrites. Right: With ferrites.

Table 3 lists, for both simulated cases, the power losses per magnet and ferrite, and the power losses in the plasma. The numbers correspond to the average losses under the assumption of a duty cycle of 6%.

Table 3: power losses for an unshielded NdFeB magnet for $f = 2\text{MHz}$, $I_{peak} = 350\text{A}$, and 6% duty factor.

	P_{diss} [W]		
	magnet	ferrite	plasma
Without ferrites	72	-	573
With ferrites	31	1×10^{-5}	640

The simulations show that power losses are high in the magnets during SPL operation. Even if ferrites are used, P_{diss} is in the range of several tens of Watts at

6% duty cycle and would likely result in magnet temperatures above the Curie temperature T_{Curie} . With ferrites, the power losses in the magnets are reduced by more than a factor of two, and power dissipation in the plasma is higher since the ferrites increase the magnetic flux in the plasma region. For the ferrites themselves ohmic losses do not pose a problem since their low conductivity effectively suppresses the generation of eddy currents. However, the influence of hysteresis losses remains to be investigated.

The results indicate that it is necessary to shield them with a material with higher conductivity (e.g. Cu) in order to minimize the ohmic losses in the magnets. To assess the improvement due to the shielding, Opera simulations of an advanced system were performed which resembles the setup before but has the magnet covered by 0.5mm of Cu (Fig. 21). This thickness corresponds to ≈ 10 skin depths of Cu.

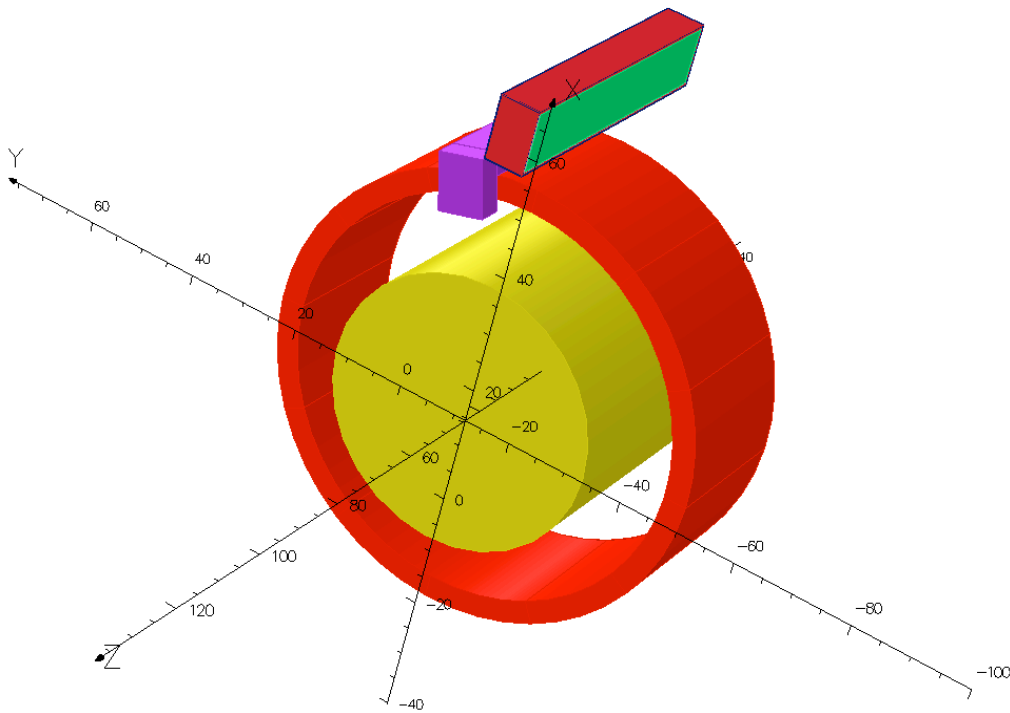


Figure 21: Simplified model of the SPL plasma generator with Cu-shielded magnets. Red: RF antenna. Yellow: plasma cylinder. Green: NdFeB magnet. Purple: Ferrite. Dark red: Cu shielding.

The results of the simulations are summarized in Table 4. Clearly, the power dissipated in the Cu shielding is more than one order of magnitude smaller than in an unshielded NdFeB magnet. Moreover, the power dissipated in the magnet itself is negligible, illustrating the positive influence of the Cu shielding.

Table 4: power losses for a Cu shielded NdFeB magnet for $f = 2\text{MHz}$, $I_{peak} = 350\text{A}$, and 6% duty factor.

	$P_{diss} [W]$			
	Cu shielding	magnet	ferrite	plasma
Without ferrites	4.8	6×10^{-6}	-	572
With ferrites	2.1	5×10^{-6}	1×10^{-5}	639

Design and production of the SPL plasma generator magnet cage

The results of the Opera simulations triggered the development of a magnet cage that is entirely made of Cu. A 3D drawing of the final design and a photograph of the produced piece are shown in Fig. 22. The cusp magnets are contained in rectangular holes with a cross-section of $14.2 \times 10.5 \text{ mm}$. Small wedges installed at the back end of the holes after magnet insertion prevent the magnets from falling out. The magnets are pushed inwards by plastic screws, assuring that the magnetic cusp field is as homogeneous as possible and not disturbed by any misalignment of the magnets. The magnet cage is closed at the front end by a Cu ring brazed onto the main body of the magnet cage. This Cu ring contains small holes at the position of each magnet which allow pushing them backwards when the magnet cage is disassembled. The external surface of the magnet cage contains additional screw holes which allow for mounting an optional cooling system on the outside, in the case that active cooling of the magnet cage is required during high average power operation. A cut out at the back end provides access to the plasma chamber cooling outlet.

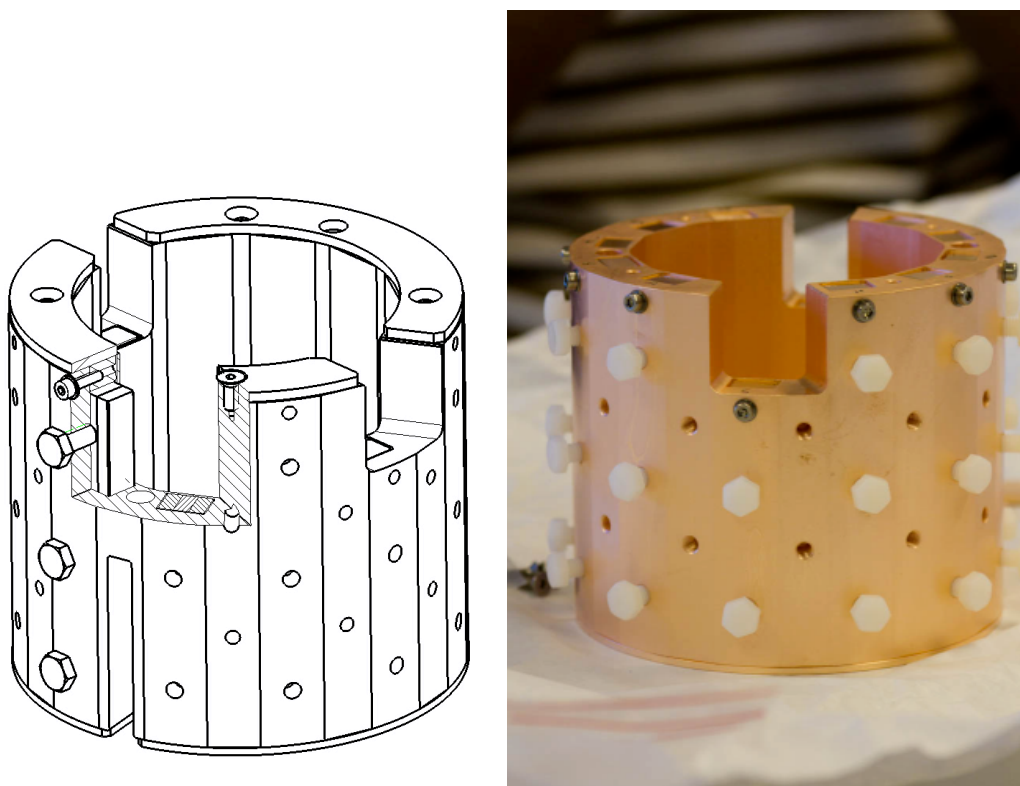


Figure 22: SPL plasma generator magnet cage. Left: 3D technical drawing. Right: photograph.

A total of three different magnet sets have been purchased from two different suppliers. The brick-shaped magnets and eight Halbach elements were purchased from Vacuumschmelze ³ (material: Vacodym 633HR). Additional 18 Halbach elements were purchased from IMA ⁴. The different sets are listed in Table 5.

Table 5: Available cusp magnet sets and remanences B_r .

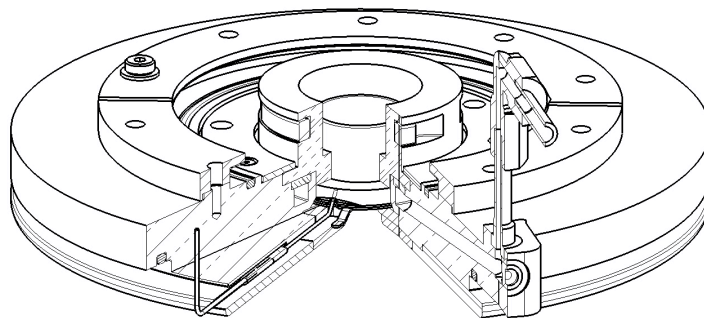
material	producer	B_r [T]	magnetization	Size [mm ³]	# pieces
Vacodym 633HR (NdFeB)	Vacuumschmelze	1.35	N-S	13.5 x 10 x 99	18
				13.5 x 10 x 71	4
			Halbach	(3 x 4.5) x 10 x 99	8
Nd 38 (NdFeB)	IMA	1.26	Halbach	(3 x 4.5) x 10 x 99	14
				(3 x 4.5) x 10 x 71	4

5. Sub-assembly C: extraction region

General outline

A 3D view of the extraction region is shown in Fig. 23 alongside with a photograph of the produced piece. The main differences between the extraction region of the SPL plasma generator and its Linac4 counterpart are: The removal of the tilting collar; the use of AlN ceramic for electrical insulators; and the brazing of the molybdenum funnel and aperture electrodes with the insulators that separate them from each other and from the metallic body of the plasma generator (Fig. 24). All these changes serve to optimize the heat transportation away from the collar electrodes.

The filter magnets are contained in an AlN magnet holder. Unlike the filter magnets used in the Linac4 source, the magnets of the SPL plasma generator are arc-shaped to minimize the required space, and to achieve a better radial uniformity of the magnetic filter field. Three different sets of filter magnets are available for testing (see Table 6).



³ Vacuumschmelze GmbH & Co. KG, Grüner Weg 37, D-63450 Hanau, Germany

⁴ IMA Ingeniería Magnética Aplicada S.L., Avda. Rafael Casanova, 114, 08100 Barcelona, Spain

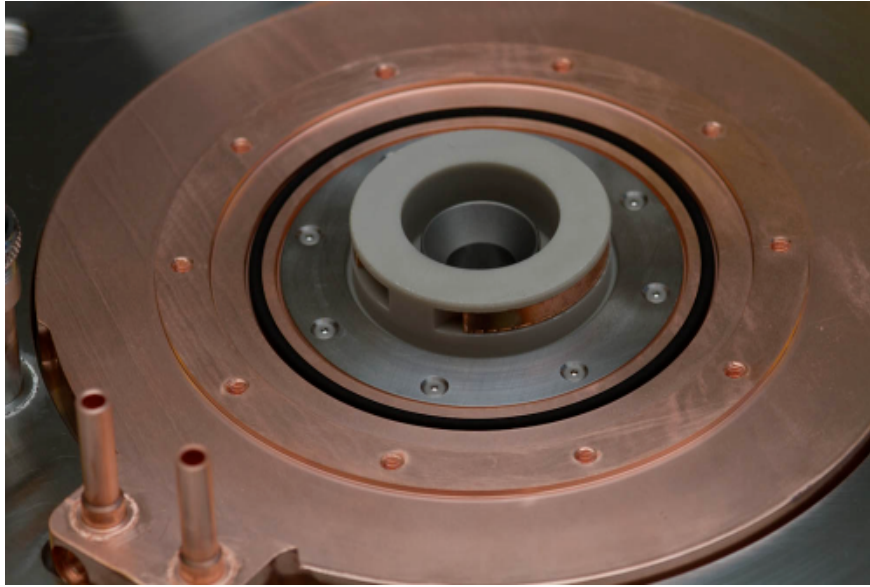


Figure 23: Extraction region. Top: 3D CAD view. Bottom: Photograph of the produced piece.



Figure 24: Brazed electrode assembly consisting of the funnel and aperture electrodes, the separating AlN insulators, and the electrical connections.

Table 6: Available filter magnet materials and remanences B_r .

material	Type	producer	B_r [T]
Vacodym 633HR	NdFeB	Vacuumschmelze	1.35
Vacodym 677HR	NdFeB	Vacuumschmelze	1.18
Vacomax 170HR	SmCo ₅	Vacuumschmelze	0.95

Design changes since the previous deliverable report

Only minor design changes were done on the extraction region since the previous report. The outline of the collar electrodes and adjacent insulators was changed slightly in order to facilitate the electrical connections of the electrodes. The magnet holder design was slightly altered according to suggestions by the producer (CeramTec). The size of the filter magnets was reduced, and Cu containers designed in order to protect them from overheating by RF induced eddy currents. Finally, the radial dimensions of the adapter plate were increased to account for the larger dimensions of the PEEK cooling sleeve and the magnet cage, and the material changed to Cu in order to optimize heat transportation.

5.1. Opera modeling of the filter region

As the cusp magnets, the filter magnets are located in a region with high B field strengths and ohmic heating can cause problems during operation with high RF power and high duty factors. For this reason, the eddy-current induced dissipation of RF power in the filter magnets was equally modeled by a simplified EM model. All materials were modelled as in the cusp magnet simulations (Sect. 4.6). Simulations were performed with and without ferrites around the antenna. Both unshielded and Cu-shielded filter magnets were considered. As before, the thickness of the Cu shielding was set to 0.5mm.

Fig. 25 shows the simulated B field distribution in the vicinity of an unshielded filter magnet. The B field seen by the magnet (and therefore, the losses) is highest at the surfaces that are closest to the antenna.

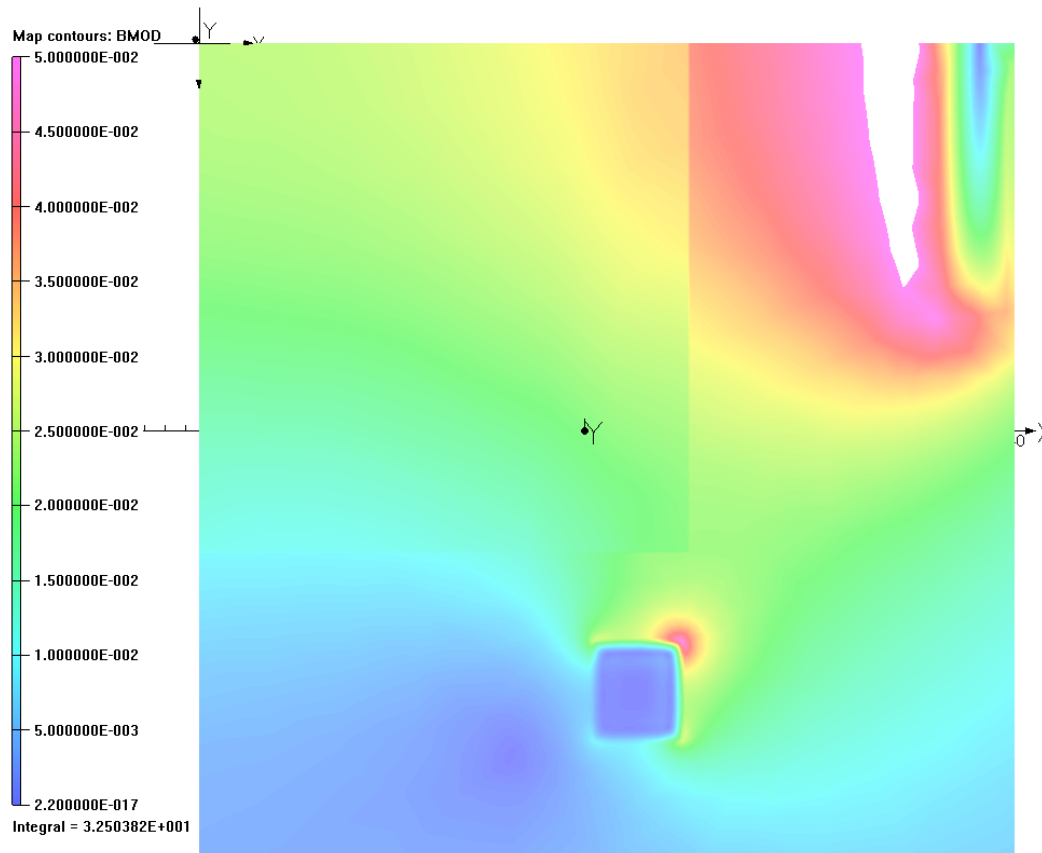


Figure 25: B field distribution in the vicinity of the filter magnets.

The results of the different simulation runs (with/without ferrite, no shielding/Cu shielding) are compared in Table 7. Without Cu shielding and ferrites, 40W are dissipated in each filter magnet on average at 6% duty factor, likely leading to overheating of the magnets. This number is only slightly reduced by the ferrites since their impact on the field strength in the vicinity of the filter magnets is only small. However, as for the cusp magnets, the results show that the dissipated power is reduced by more than one order of magnitude if the filter magnets are shielded by Cu. As a consequence, small Cu boxes were produced to protect the filter magnets (Fig. 26).

Table 7: Power losses in filter magnets for $f = 2$ MHz, $I_{peak} = 350$ A, and 6% duty factor.

Ferrites	Cu shielding	Filter magnet	P_{diss} [W]	
			Cu	ferrite
no	no	40	-	-
yes	no	36	-	1×10^{-5}
no	yes	6×10^{-6}	2.8	-
yes	yes	5×10^{-6}	2.5	1×10^{-5}

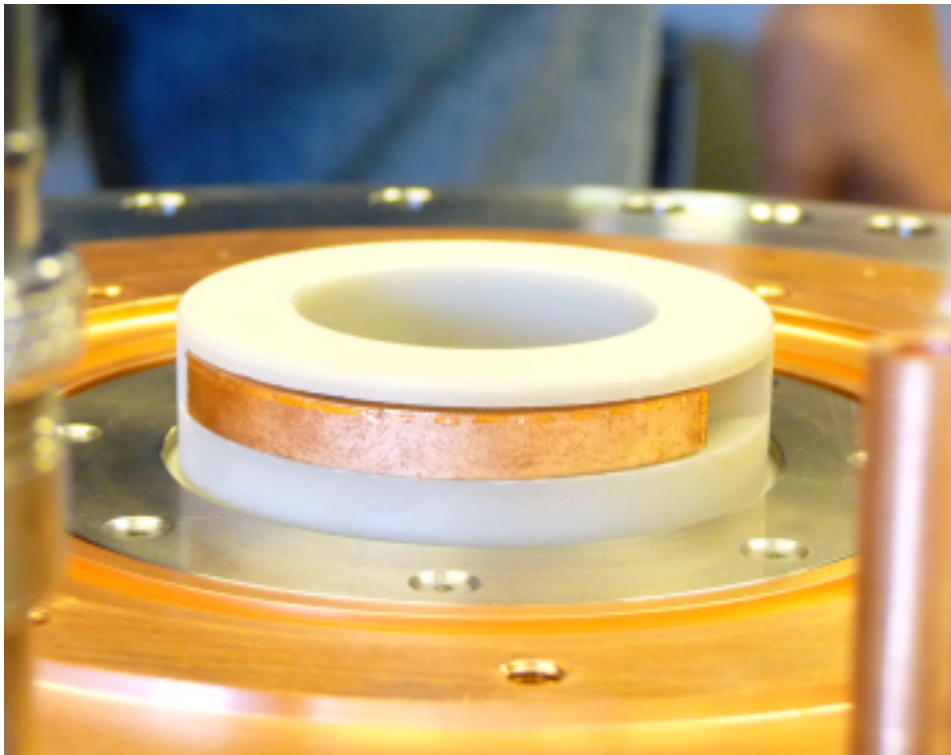


Figure 26: Cu shielded filter magnet.

6. Sub-assembly D: mechanical support

General outline

A 3D view of the mechanical support is shown in Fig. 27. The mechanical support consists of a DN-200 flange connected to a DN-150 for installation at the test stand, a tripod stainless steel structure, and a back plate.

6.3.1. Design changes since the previous deliverable report

The most important changes include the use of a DN-200 flange instead of a DN-150 due to the increased space requirements for the plasma chamber sub-assembly. The plasma generator is clamped onto the DN-200 flange at the front end. Further positioning and fixation of the plasma generator components in axial and radial direction is made possible by a series of screws and shims (Fig. 28).

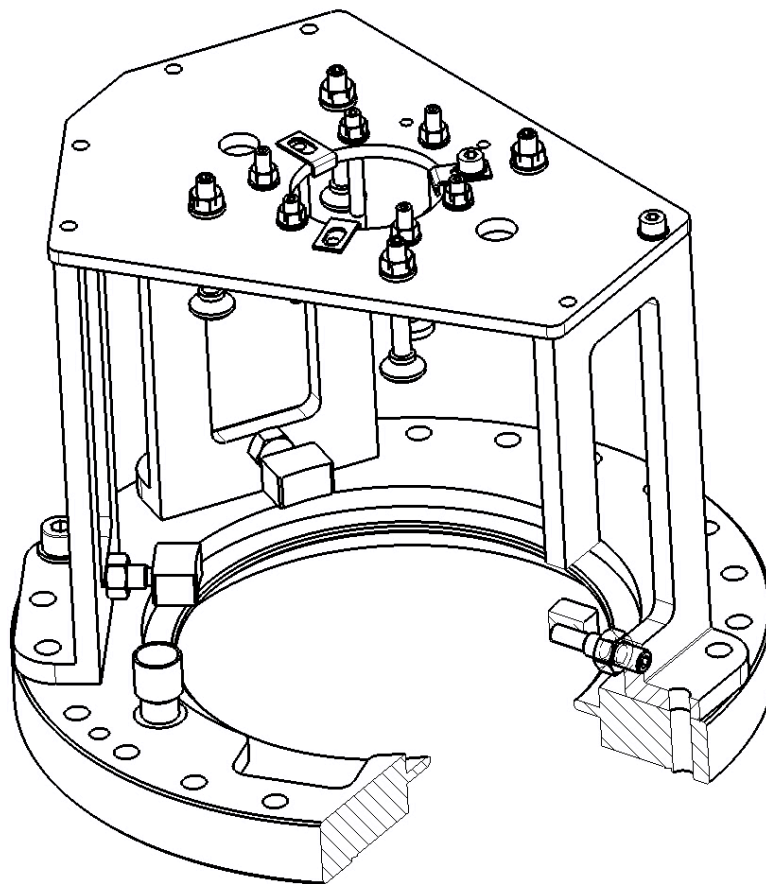


Figure 27: 3D view of the mechanical support of the SPL plasma generator.

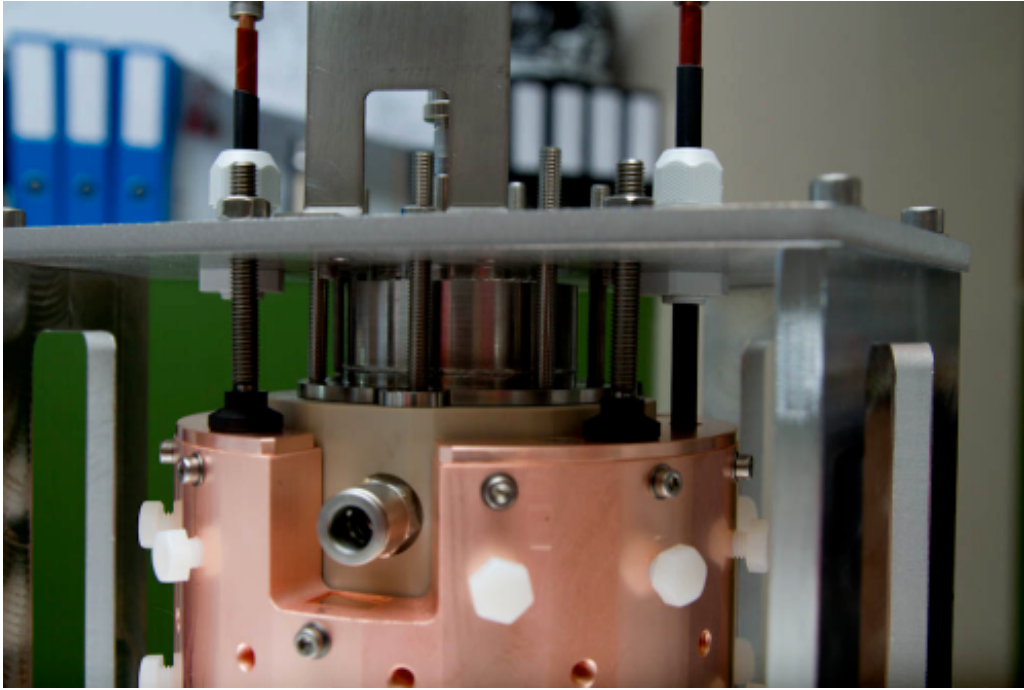


Figure 28: Fixation screws for the plasma chamber, PEEK cooling sleeve, and the magnet cage.

7. Plasma generator cooling systems

The SPL plasma generator involves a total of five cooling systems which have been designed according to the cooling requirements of the individual components (see [5]). Their properties are summarized in Table 8. All cooling circuits have been leak tested prior to installation of the plasma generator at the test stand.

Table 8: Summary of cooling systems.

Sub-assembly/component	Flow rate [l/min]
Plasma chamber	3
H ₂ gas injection and ignition	0.5
Collar region	2
RF antenna	0.5

8. Test stand

The general layout of the SPL plasma generator test stand in room 357-R-005 is sketched in Fig. 29. In the following sections, the experimental setup is presented.

Vacuum and Gas: The high pressure hydrogen, nitrogen and argon gas cylinders are located outside the building. The low pressure gas distribution and experimental vacuum chamber are classified as explosive risk areas and constantly monitored via hydrogen calibrated gas detectors. The gas distribution, high voltage power transformer and RF generator are interlocked by the flammable gas detection system.

Three pumping systems are installed:

- A mobile system dedicated to the rest gas analyzer (60 l/s turbo molecular pump and roughing pump)
- Low pressure gas distribution (60 l/s turbo molecular pump and roughing pump)
- Experimental chamber (500 l/s with the option to add a 60 l/s turbo molecular pump in series and roughing pump).

The exhausts of the experimental chamber and gas injection are evacuated on the roof of building 357.

RF Generator: the high voltage power transformer and the RF generators are installed within four racks. A single coaxial cable feeds the matching network in the vicinity of the plasma generator. The matching network itself is located within a dedicated faraday cage.

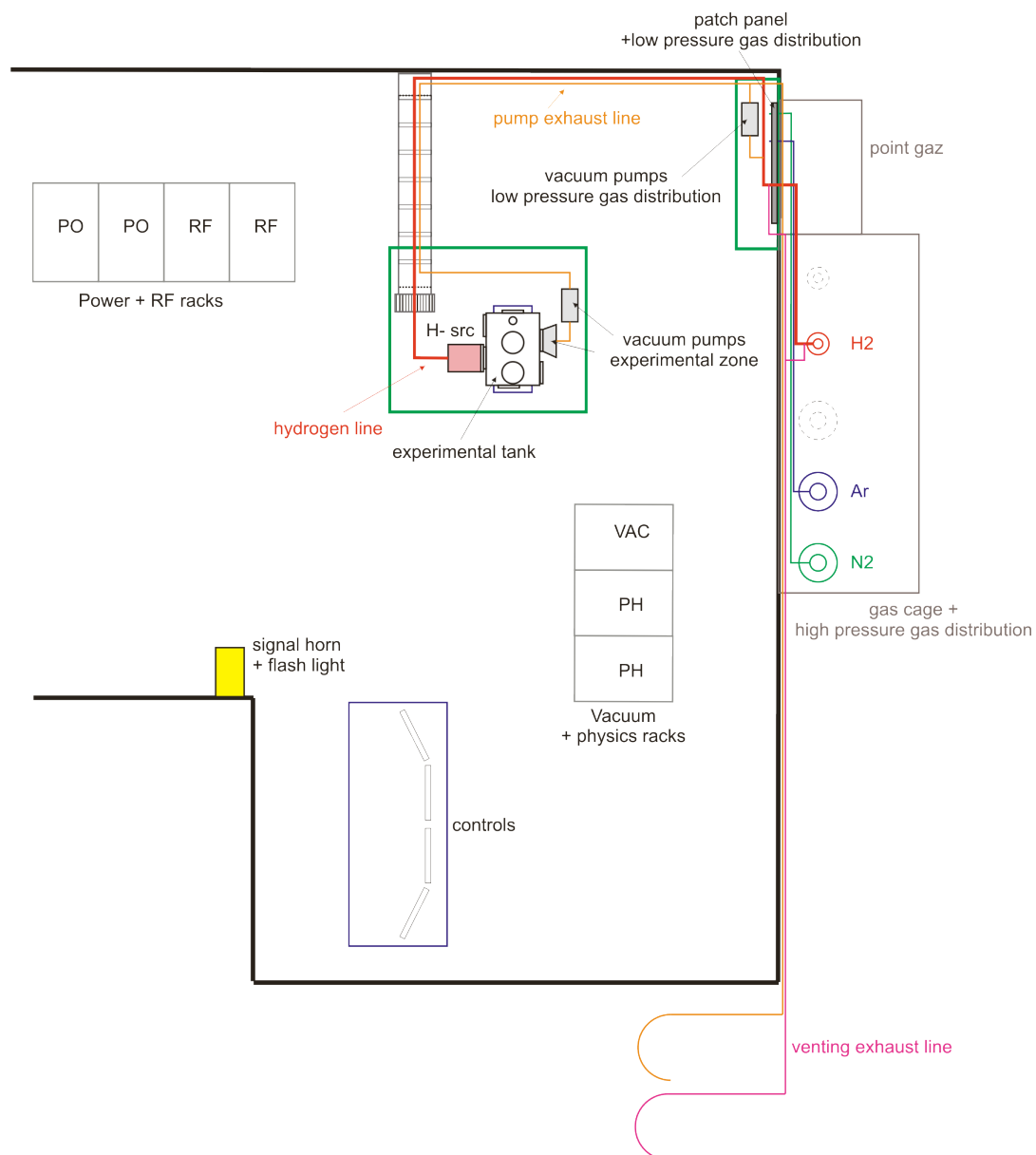


Figure 29: General layout of SPL plasma generator test stand in Room 357-R-005. The gas system, the experimental vacuum chamber, the racks for RF generation, vacuum control and measurement and triggering are indicated.

Monitoring, controls, measurements and diagnostics: two racks contain the arbitrary function and delay generators. Temperature and pressure monitoring systems are based on PLCs, Step7 and Labview. Dedicated PLCs are checking the status of the experiment, generate visual warnings, and disable the power supplies requests. A slow control database monitors all values while high frequency signals are recorded via oscilloscopes. A set of 2 PCs and four screens build the control system of the test setup. A laptop is dedicated to the measurement of magnetic field maps with a 3D Hall gauge and to the control of the rest gas analyzer. A second laptop is dedicated to the control of an optical spectrometer dedicated to the measurement of the visible light generated by the plasma (i.e. Hydrogen Balmer lines). A photo camera triggered by the control system is foreseen to record the behavior of the plasma ignition system installed onto the quartz mockup of the plasma generator chamber and to view the plasma distribution in the plasma generator via dedicated transparent extraction plate.

Temperature: the vacuum chamber, the gas and cooling circuits are equipped with Pt-100 temperature gauges to monitor the heat flow and experimental conditions. An infrared camera is available to map external surface temperatures and, via a Germanium window, also the temperature of the extraction region of the plasma generator.

8.1. Experimental vacuum chamber

The experimental chamber (Fig. 30) is a three axis cross comprising six DN-150 flanges. The plasma generator or its Quartz mockup is mounted on one of the side flanges. The opposite flange can be equipped alternatively with the rest gas analyzer, a Quartz window for visual inspection and optical and spectroscopic measurements, or a Germanium window for thermal monitoring of the extraction region.

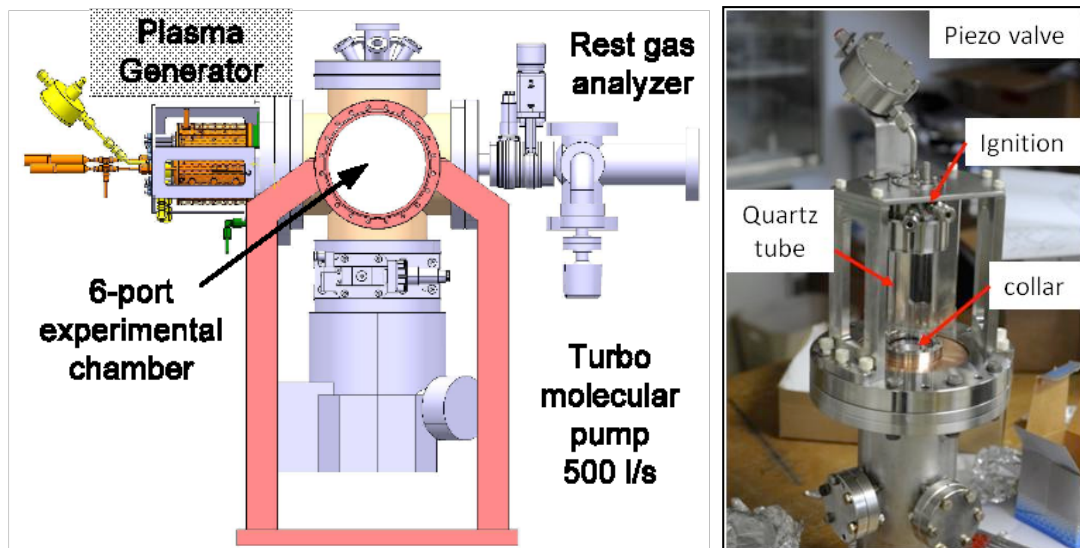


Figure 30: Scheme of the experimental chamber (left), the plasma generator and RGA are indicated. The mockup dedicated to plasma ignition studies (right) can be coupled to the experimental chamber instead of the plasma generator.

It is likely that the plasma conditions will be slightly different with and without extraction, and for extraction of positive or negative particles. If time and finances permit, a simple few-kV extraction system consisting of two Helmholtz coils to separate electrons from ions and two Faraday cups will be installed to monitor these effects.

The top flange is equipped with several gauges for vacuum diagnostics and Nitrogen injection while the bottom one hosts the turbo molecular pump.

8.2. Gas system and gas safety installations

The test stand can be run with several types of gases (N_2 , Ar and H_2). Additional spare gas lines for potential use of other gases (e.g. CH_4 and He) are available.

The gas bottles are stored outside of building 357 in a vented metallic cage. Each bottle is connected to an individual gas line that runs through the wall and ends at a patch panel close to the test stand. The gas pressure is reduced from bottle pressure to a maximum of 5 bars by a pressure reducer.

From the patch panel, the gas is redistributed to a second panel (low pressure gas distribution panel, Fig. 31) that serves as an interface between the patch panel, the experiment, and the vacuum and exhaust systems. The low pressure gas distribution panel contains, for each gas type, reduction manometers and precision pressure gauges that allow setting the gas pressure to the nominal values. Two vacuum pumps in series (1x mechanical, 1x turbo pump) can be used for emptying the gas pipes before startup, after an intervention to avoid a potential hazardous mixture of H_2 with air, or to fine adjust the gas pressure inside the gas line.

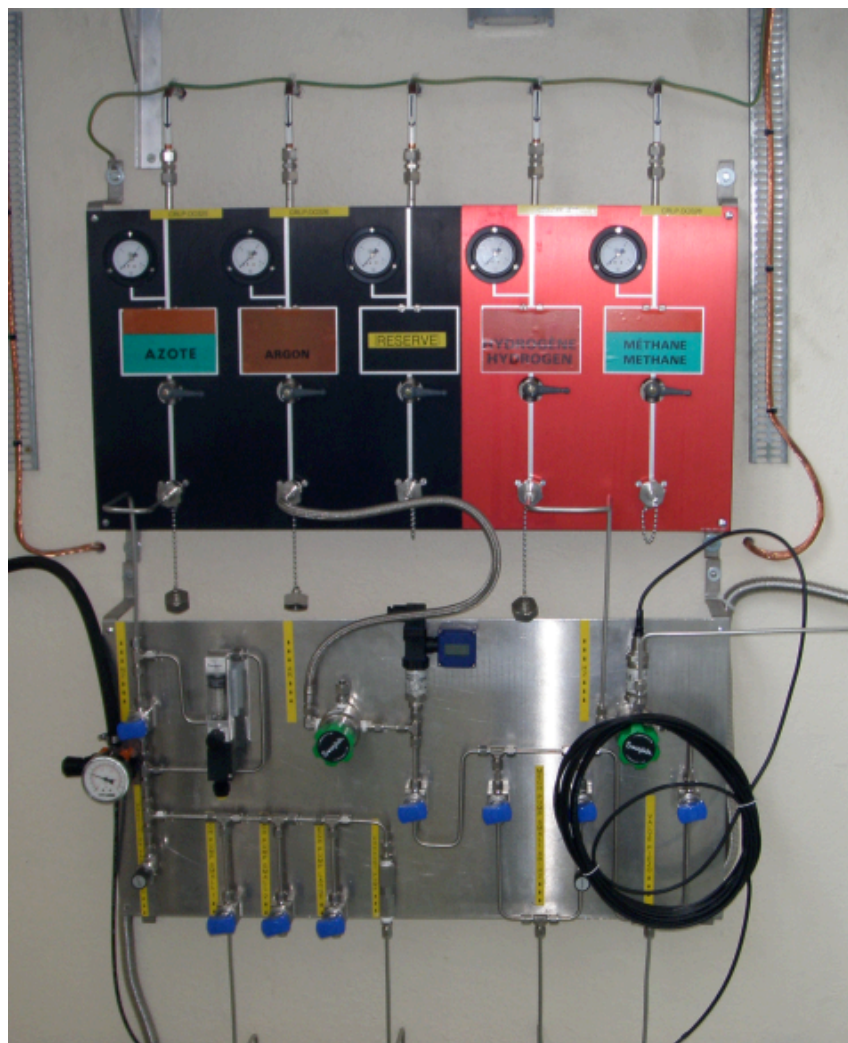


Figure 31: Gas distribution system. Top: Patch panel. Bottom: Low pressure gas distribution.

The experimental setup is supplied with hydrogen or Argon via a single stainless steel pipe that is coupled via a flexible stainless steel tube to the piezo valve of the plasma generator. Furthermore, the experimental chamber vacuum tank can be filled with N₂ through a dedicated gas line limited to atmospheric pressure.

Several gas safety systems have been installed and commissioned at the test stand in order to minimize the risk of a hazardous event involving flammable H₂. H₂ gas pumped by the vacuum pumps or released through the overpressure valves is transported away by two exhaust lines that end at the roof of Bt. 357. The pump exhaust line is constantly flushed with N₂ to ensure a non explosive N₂-H₂ gas mixture.

Two flammable gas detectors (type OLC-50) are installed in metallic hoods above the gas panels and the experimental zone. Both are coupled to a central unit (MX-32) that triggers a gas alarm in the case of a potentially hazardous H₂ concentration. The interlock scheme applied in case of a gas alarm is depicted in Fig. 32.

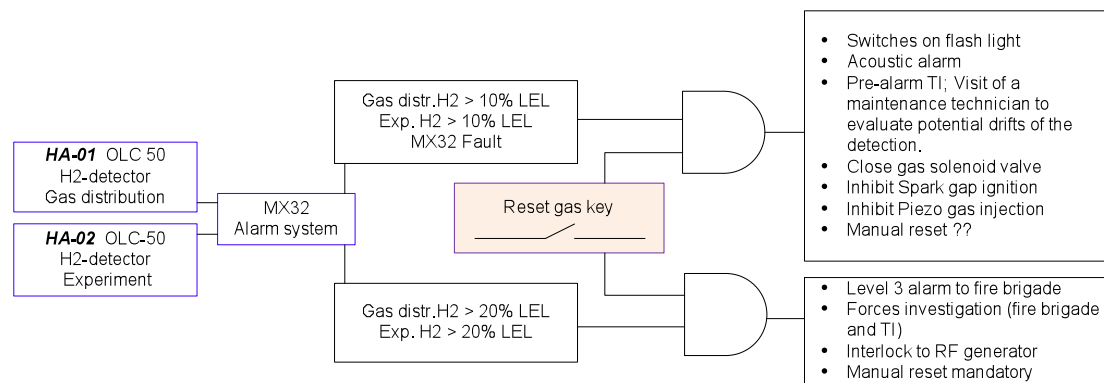


Figure 32: Interlock scheme for H₂ operation. The Lower Explosive Limit (LEL- H₂ = 3.5% vol. in air) is used to set maintenance warning (10% LEL) and alarms coupled to the interlock circuit (20% LEL).

Additional hardware protection interlocks disabling RF and ignition pulses are triggered if the temperature of the cooling water rises above a certain threshold, or, if the coolant flow is below the lower threshold for any of the cooling circuits (Fig. 33).

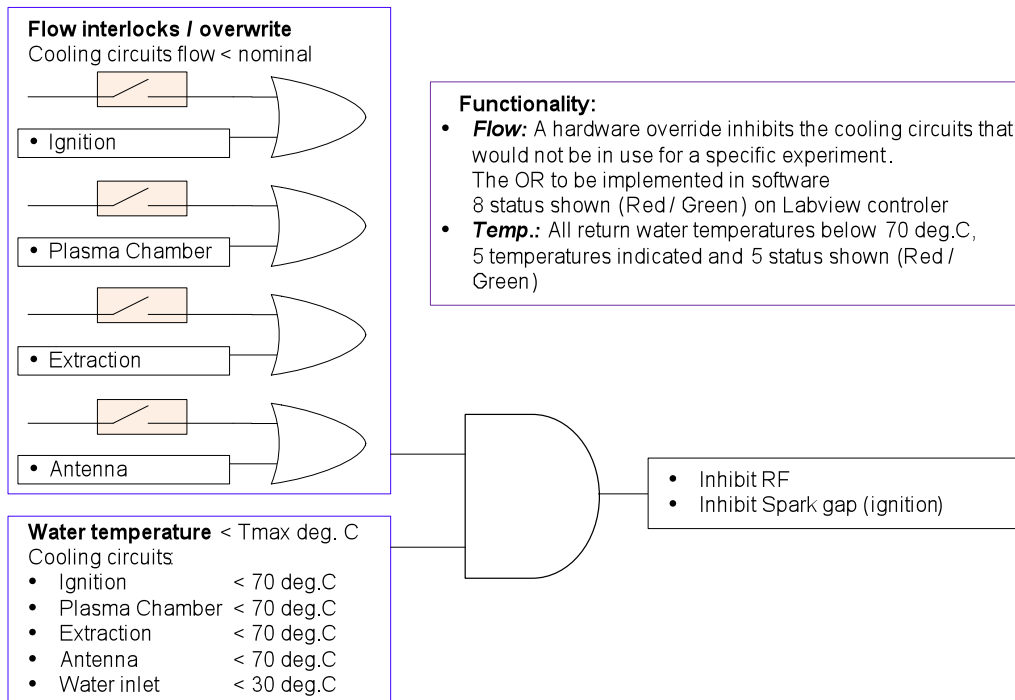


Figure 33: Interlock scheme for the plasma generator cooling system. A hardware bypass of individual cooling circuits can be set manually (i.e. operation with the mockup).

8.3. Vacuum system

Experimental Chamber: The top flange is equipped with three complementary gauges for pressure measurement with 5% to 10% precision from high vacuum ($p \approx 10^{-8}$ mbar) to atmospheric pressures. The vacuum gauges were selected with overlapping measurement ranges as follows:

- APR 260, 0.1 -1100 mbar, Pfeiffer Vacuum
- CMR 275, $1 \cdot 10^{-5}$ -0.11 mbar, Pfeiffer Vacuum
- PBR 260, 10^{-8} - 10^{-2} mbar, Pfeiffer Vacuum

The gauges are controlled with a MaxiGauge TPG 256 A unit from Pfeiffer Vacuum which allows simultaneous reading of the three gauges. The bottom flange is equipped with a turbo pump (500 l/s, Pfeiffer TMU-521) in series with a Ex-rated mechanical pump (Edwards 12). Both pumps are controlled with one single pumping control unit (CERN-PS standard).

Low pressure gas distribution: The low pressure gas distribution patch panel feeds a low conductivity Piezo valve, aA pre-vacuum is mandatory to minimize gas impurities. Due to the location in a hazardous area, an oil-based EX-rated mechanical pump (Edwards 12) was chosen. In order to assure cleanest possible conditions, a small turbo molecular pump (60 l/s, Pfeiffer TMU-071) was implemented.

Quadrupole mass spectrometer for rest gas analysis and plasma process monitoring (rest gas analyzer): The QMA 125 is a bake-able UHV standard equipped with a small turbo molecular pump (60 l/s, Pfeiffer TMU-071) and a mechanical pump (Edwards). It will be connected to the experimental chamber via a retractable aperture reduction and a metallic valve.

8.4. Cooling and temperature control systems

Plasma chamber: The five cooling systems of the plasma chamber are presented in Fig. 34. The injection and individual return water temperatures are measured via dedicated Pt-100 resistors. Individual flow interlocks are installed on each cooling circuit. The system was successfully commissioned.

Piezo valve: The temperature of the piezo valve is controlled by an industrial closed loop controller (LAUDA Alpha RA8) to a precision of 0.1°C. This should ensure stable conditions and the study of its dependence on seasonal or day-night room temperature fluctuations.

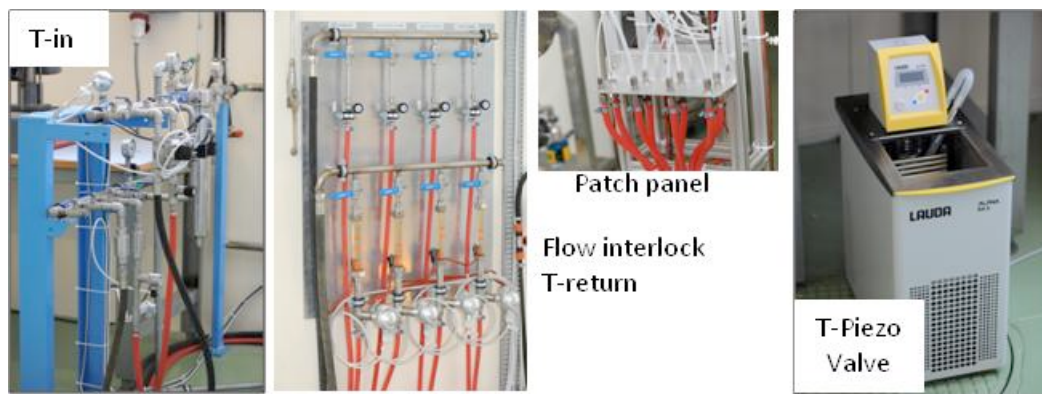


Figure 34: Views of the water cooling system. From left to right: the demineralized water distribution, the flow interlock and temperature measurement, and the patch panel leading to the individual plasma chamber circuits. The temperature controller of the piezo valve is shown in the rightmost image.

8.5. HT-power converter and RF generator

The RF generator [7] is shown in Fig. 35, it has to provide 100kW, 2MHz bursts of up to 1.2ms duration at a 50Hz repetition rate for the plasma heating. The system is designed as an upgraded version of the one installed at Linac4. The higher duty cycle imposed by the increased repetition rate (50Hz vs. 2Hz) and increased pulse duration (1.2ms vs. 0.4ms) required upgrading the 22kV HV power supply and overall system cooling. The complete system including the power supplies, RF low-power and high-power sections, interlocks and timings has been built, installed and tested on a 50Ω load at nominal parameters. A high directivity directional coupler present at the power stage output allows measuring the forward and reflected waves from which the contribution of the plasma to the circuit's impedance can be deduced. A servo loop controlling the forward power as well as frequency hopping ability will allow optimization of the power transmitted to the plasma despite the impedance variation at plasma ignition.



Figure 35: Left: High voltage and 2MHz RF generator. Right: Vacuum and controls racks.

8.6. Faraday cage and RF matching network

The Faraday cage encloses the plasma generator and the RF matching network. A 3D view of the assembly is shown in Fig. 36. A view port is foreseen for temperature measurements of the Cu-magnet housing with an IR camera (Fluke Ti32).

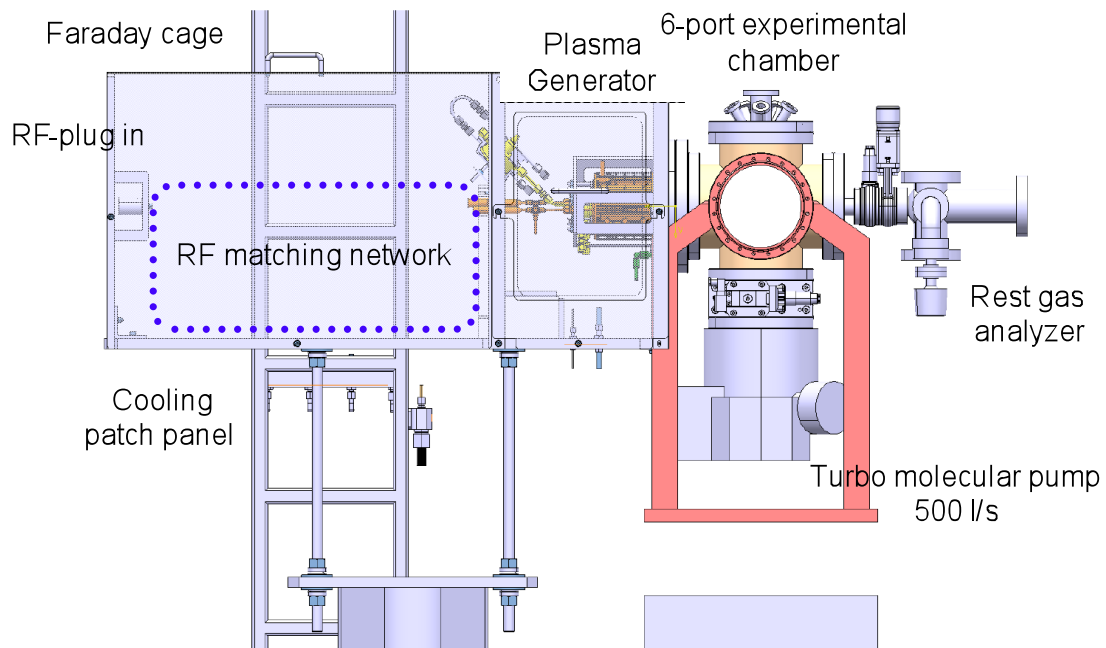


Figure 36: The faraday cage enclosing the plasma generator and the RF matching network is positioned onto the experimental vacuum chamber. The turbo molecular pump and, as an example of a plasma diagnostic device, the rest gas analyzer are shown.

8.7. Plasma ignition and piezo valve pulsed power supplies, collar and Plasma extraction plate power supplies

The ignition pulser supply (Fug MCP 140-1250) delivers a pulse of up to 1000V limited to 10A for a duration of up to 100 microseconds at a maximum rate of 50Hz. A +1000V DC supply is backed by capacitors, the output is switched using a high voltage bipolar MOSFET. A selectable series resistor limits the output current.

The Piezo valve is driven by a in house assembled power supply capable of delivering -10V to +100V. The power supply has two inputs which are both amplified 20x then summed. Using an arbitrary waveform generator on one input and a DC level on the other any combination of DC offset and pulse shape is possible to drive the valve.

The Plasma extraction plate and Collar electrode supplies are identical and consist of a Fug NTN 140-65 +/-65V 2A DC supply. The output of the power supplies is backed by a 22000 μ F capacitor to allow a peak current of 10A for 1.2ms during the beam pulse and to limit the voltage droop to 2% when operated at 30V.

8.8. Plasma diagnostics

The SPL project's focus is in the production of a system capable of enduring 2 orders of magnitude more RF power than the ion source operated at Linac4 nominal parameters. The equilibrium temperatures will witness this achievement. However, the plasma parameters (plasma potential, electron and ion densities and temperatures) of an H⁻ ion source are usually tuned to maximize the H⁻ current and minimize its emittance as well as the co-extracted electron current. It is important to characterize the plasma of the SPL plasma generator and whenever possible to compare it to the one of the operational Linac4 ion source. For this purpose, the following devices for plasma diagnostics will be used:

Optical spectrometry: spectrometry of visible light emitted by the plasma's Hydrogen Balmer lines (Ocean Optics 4000) with fiber optics connection. A database of elemental and molecular emission lines shall also allow tracking down of plasma impurities but also emission from the ceramic walls.

Rest gas analyzer: the QMA 125 can be operated for gaseous element but also in plasma monitoring (ion and neutrals) mode whenever placed in direct view of the plasma.

Langmuir gauge or ion retardation methods are the key to the plasma potential. The Langmuir gauge is a priori the most established method. Positioned through the extraction hole it should allow measuring the plasma potential. The emerging retardation method should allow a time resolution of the plasma potential and wise no perturbation of the plasma. However, this method requires an extracted beam.

RF-coupling: the contribution of the plasma to the impedance of the matching circuit is expected to characterize the energy transferred into the plasma and will be studied. Its sensitivity to standard plasma parameters is not yet established, however, it will be used as a comparative tool between the Linac4 and SPL plasma generators.

8.9. Timing, Slow control and data storage

The test stand involves a data acquisition (DAQ) system for slow control and processing and storage of experimental data. A schematic outline of the DAQ system

is shown in Fig. 37. It involves input and output modules connected to a PLC with Step7 configuration for data processing, and a Labview program that monitors and stores the data from the sensors and controls the interlock system and gas valve offset.

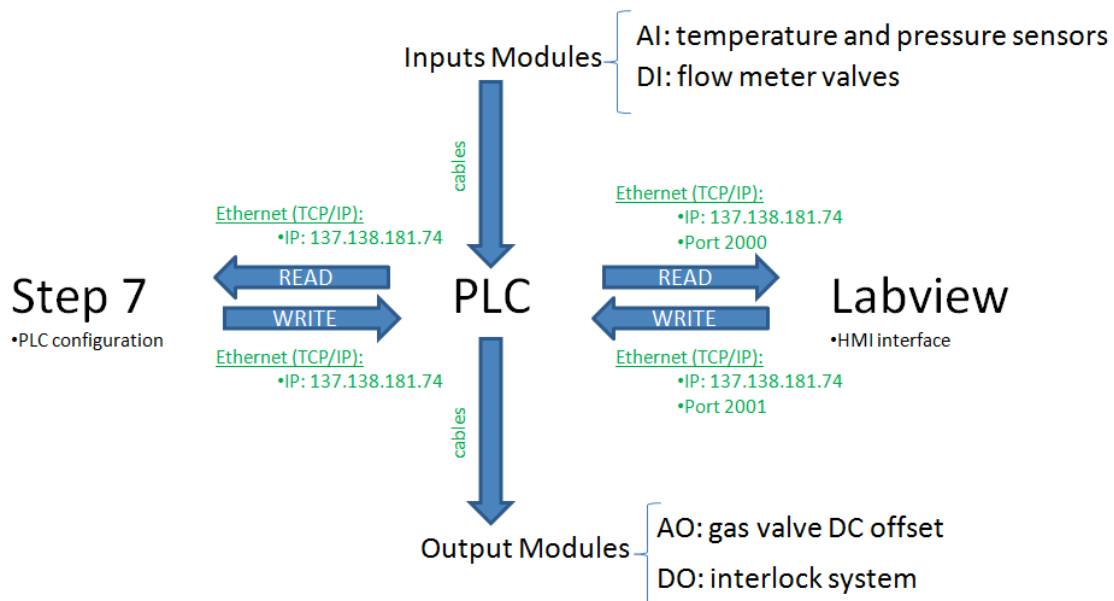


Figure 37: Outline of the Step7 and Labview based slow control data acquisition chain.

The following parameters are constantly monitored:

- Pressure of the Hydrogen and Argon low pressure injection
- Pressure inside the vacuum tank (3 vacuum gauges)
- Temperature of the piezo valve
- Temperature and flow rate of the cooling water

If one of the read values is out of the nominal range, the Labview program activates the inhibit system, interrupting the experiment and switching off the piezo valve, plasma ignition, and extraction collar power supplies. Furthermore, a visual signal is displayed on the Labview console.

The timing of the experiment is based on two 8-channel pulse generators (QI-9520). One pulse generator is dedicated to triggering of all power supplies involved in the plasma generation (piezo valve, plasma ignition, RF antenna, extraction collar). The second pulse generator is used to synchronize the measurement systems (oscilloscopes, rest gas analyzer, photo camera, and optical spectrometer). An outline of the timing system is presented in Fig. 38.

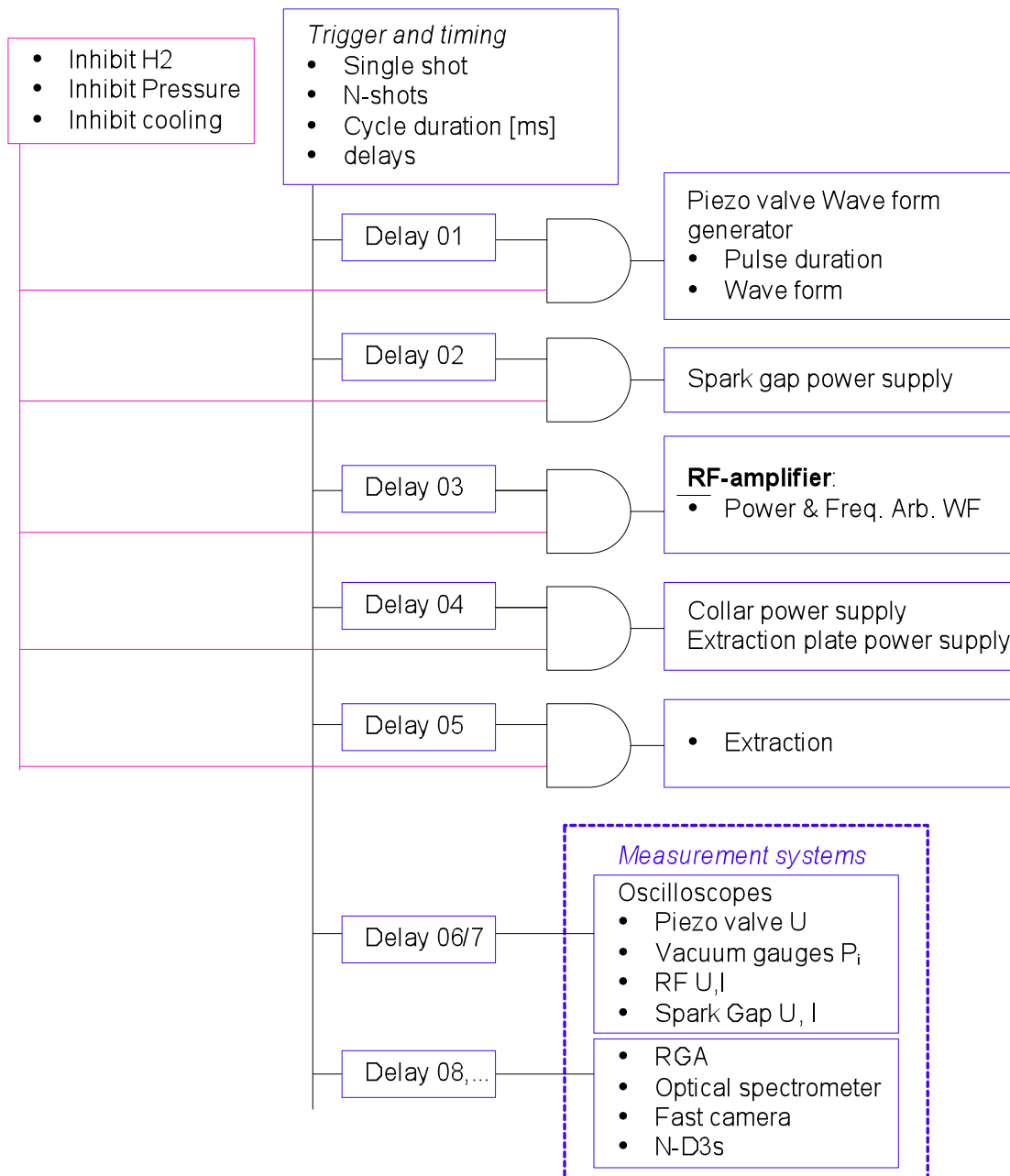


Figure 38: Triggering system of the plasma generation and fast data acquisition.

9. Conclusion and outlook

A prototype of the SPL plasma generator has been produced, successfully leak tested and installed onto its test stand. The last engineering item, namely the protection of the permanent magnets from RF induced eddy current heating, was addressed. A test is foreseen to support the estimations. All installations and documents related to gas safety have been completed. The test stand vacuum and gas systems, the gas injection and the plasma ignition have been commissioned. Remaining are the acceptance test of the new electrical installation (i.e. grounding), and the Faraday cage that is being produced and will be installed early October.

A risk analysis on the plasma generator components pointed out that the most critical item in terms of machining and resilience to high power operations is the AlN ceramic plasma chamber. Indeed, the two units produced so far by the supplier did not fully

match our specifications, and one of the units was damaged during assembly. An additional effort is therefore required to ensure conformity of this ceramic.

The next months will be dedicated to thorough testing of the prototype to demonstrate its compliance with the sLHC-PP specifications. The measurements of plasma parameters will be compared to those of the Linac4 ion source's plasma via the RF coupling and light emission in order to assess similarities with an operating ion-source.

Acknowledgements: the authors are grateful and wish to acknowledge the contributions and support from: Laszlo Abel, Alessandro Bertarelli, Oliver Bruning, Maryse Da Costa, Alain Demougeot, Paolo Chiggiato, Ramon Folch, Philippe Frichot, Roland Garoby, Jonathan Gulley, Christophe Jarrige, Erk Jensen, Emmanuel Koutchouk, Robert Mabillard, Marina Malabaila, Cristiano Mastrostefano, Sophie Meunier, Oystein Midttun, Catherine Montagnier, Jose Monteiro, Mauro Nonis, Julien Parra-Lopez, Stephen Rew, Miguel Riesgo Garcia, Ghislain Roy, Franck Schmitt, Alain Stalder, Laurent Tardi, Dominique Trolliet, Donatino Vernamonte and Fredrik John Carl Wenander.

10. References

[1] D. K uchler, T. Meinschad, J. Peters, R. Scrivens, A radio frequency driven H⁺ source for Linac4. Rev. Sci. Instr. 79, 02A504 (2008)

[2] M. Kronberger, R. Scrivens, J. Lettry, Finite element thermal study of the Linac4 design source at the final duty factor. SLHC WP 7.1.1 Deliverable report, 03/2009

[3] D. Faircloth, M. Kronberger, D. K uchler, J. Lettry, R. Scrivens, Rev. Sci. Instr. 81, 02A722 (2010)

[4] D. Faircloth, M. Kronberger, J. Lettry, C.-M. Schmitzer, R. Scrivens, List of required improvements for the design of the high duty factor plasma generator to function at 6% duty factor. SLHC WP 7.1.1 Milestone report, 06/2009

[5] E. Chaudet, D. Faircloth, G. Favre, J.-M. Geisser, M. Kronberger, J. Lettry, S. Mathot, O. Midttun, P. Moyret, C.-S. Schmitzer, R. Scrivens, D. Steyaert, Design of a high duty factor plasma generator. SLHC WP 7.1.1 Deliverable report, 09/2009

[6] J. Lettry, M. Kronberger, R. Scrivens et al., Rev. Sci. Instr. 81, 02A723 (2010)

[7] HT-RF generator internal reports:

- H- Source RF Block diagram; EDMS Number 1075006
- H- Source timing and AVC CTL; EDMS Number 1075004
- 2 MHz Amplifier; EDMS Number AB-002366
- H- Source AVC; EDMS Number 1075003
- 22kV SPL Converter; EDMS Number 1095070